Thank you for spending your time on my manuscript and giving the opportunity to revise it. According to the reviews' comments and suggestions, we revised the paper carefully and tried to give satisfactory answers to the reviewers' questions. The summaries of the revision for this paper are as follows:

First, we pointed out the basic requirements of the method, and explained the reason why the method is robust to support a comprehensive geometric assessment and the possibility of applying this method to other regions or periods. Furthermore, we pointed out the limitations of the method that it cannot apply to homogeneous surfaces in the Conclusion. Additionally, we clearly stated the main aim of the paper in the revised Title and Abstract.

Second, the meaning of the Y-axes of Figure 5, 6, and 7 was clarified in the new manuscript.

Third, the changes in correlations along the simulated shifts in the along-track and across-track directions are presented. It is proved that the changes in correlations is related to the proximity of the simulated displacement to the actual displacement of the patch (taken from AVHRR GAC scene).

Fourth, the elevations of ROIs has been added in the Table 2, 3, and 4 based on SRTM Digital Elevation Data.

Fifth, some details, including the references, grammar, ROI labels, figures, as well as their captions, have been revised according to the reviewers' suggestion.

We sincerely think this study has the potential and practical values to be introduced to the readers. We really hope you could consider this paper and we believe that this study will brought new insights towards a more precise geolocation accuracy assessment, particular for coarse-resolution satellite data.

Thank you very much for your attention and consideration. For the specific comments for each reviewer, we have made detailed reply as following:

Response to Referee #1

Thank you for spending your time on my manuscript and giving the opportunity to revise it. And we also thank you for your valuable comments as they actually improve the paper's quality. In this document, we describe how we address the reviewer's comments. The reviewer's comments are marked in black color, however, our reply is marked in blue color.

SUMMARY: This study assessed geometric accuracy of global coarse resolution satellite data sets via a Correlation-based Patch Matching Method (CPMM). This study aimed to quantify the AVHRR Global Area Coverage (GAC) at the subpixel level from three different satellite products from the NOAA-17 and the Meteorological Operational Satellites (MetOp-A and -B). This study selected multiple study regions to evaluate the potential influence factors such as satellite zenith angles, latitude, longitude, and elevation. The findings of this study supported that CPMM succeeded in quantifying uncertainties of in different satellite data and identifying key influence factors/sources in their uncertainties. However, there is a major comment about the robustness of this method for more other cases. In this study, this method was evaluated for the single dates (August 13, 2003 for NOAA-17 and March 12, 2017 for MetOp-A and -B). Based on the results from a single date, the robustness of this method is still in question. As authors mentioned in the manuscript (line 34-36), an advantage of AVHRR sensors is that they have a long-term data since 1980s, which enables us to analyze it at the climate time scales. The findings of this study is more likely a case study of the geometric accuracy assessment for a single satellite imagery data.

Re: We admit that this study is a case study for geometric accuracy assessment of coarse resolution satellite datasets. In fact, a comprehensive geometric assessment of AVHRR GAC dataset over a long time series is not the focus of this paper. Instead, this study aims to propose a geometric assessment method specified for coarse resolution satellite datasets. We insist that this method is novel and robust to support a comprehensive geometric assessment. This can be explained from following aspects:

1. The traditional methods do not work well with coarse resolution satellite data due to the difficulty of detecting robust features. Even for stable lake or sea shorelines, the results suffer from the errors caused by false detection resulted from the effect of mixed pixels. Furthermore, such evaluations are often limited to certain landmarks and thus cannot support a comprehensive geometric assessment. Therefore, a more appropriate method specified for coarse resolution satellite dataset should be developed to enable a more accurate and comprehensive geometric assessment. Given the difficulty of detecting GCP on a coarse resolution image, this study has brought forward a way of thinking in another view, namely simulating the displacements with the reference map at a certain step length in different directions (within the range of ±8 km), and then checking whether the image and the reference map match the best. The geometric accuracy of the image was indicated by the simulated displacement with the best correlation. The basic principle is that when the simulated displacements is equal to the geometric errors of the coarse-resolution image, the

correlation between the image and the reference map is the largest because the spatial distribution characteristics of their spectrums are completely consistent.

Considering the influence of satellite zenith angle, topography, landcovers, latitudes and longitudes on geometric accuracy, the image is divided into many patches. And the final geometric accuracy of the image was determined by statistically summarizing the measured displacements of a very large number of patches (from the image). This method has three advantages:

- It works directly on pixel values, not a certain landmark. Therefore, it does not suffer from the errors caused by false detection due to the effect of mixed pixels and is not limited to certain landmarks. Consequently, it enables a more accurate and more comprehensive geometric assessment.

- The method itself is based on correlation calculation between the image and the reference map. It is obvious that the method is not dependent on regions or seasons. As long as the reference image and the ROI satisfy certain requirements, the method can be applied to other regions (except for homogeneous surface like water and desert) and other seasons.

- Since the method can be applied continuously in space, it provides the opportunity to study the effect of the influential factors (SatZ, topography, etc.) on geometric accuracy.

2. Although the current study is based on single dates, the selected ROIs cover different latitudes and longitudes, SatZ angles, land covers, as well as varying topographies, which represent typical influential factors on geometric accuracy. The surface conditions of these ROIs are very complicated, which is similar to most of the land surfaces on earth. Therefore, it is reasonable to believe that this method is robust and can be applied to other regions comprehensively. However, it is important to note that the method cannot work well over homogeneous surfaces such as water and desert. Because in such a situation, the correlations between the patches of the image and the reference map are always similar in any simulated displacement cases. In order to clarify this point, we have explained the possibility of applying this method to other regions and clarified that the method cannot apply to homogeneous surfaces in **Line** 569-573 as "*Although this assessment was only conducted for a single scene of each satellite, the highly variable ROIs take the influential factors of geometric accuracy well into account. Therefore, the presented conclusions are transferable to other regions or seasons. However, it is noteworthy that this method is not applicable to homogeneous surface (e.g., water, desert), where the correlations are almost the same in any simulated displacement cases.*".

As mentioned by the reviewer, the advantage of AVHRR sensors is the availability of data over multiple decades. Therefore, the AVHRR GAC data should be evaluated for all NOAA and MetOp platforms throughout the lifetime of the dataset on the global scale, which is particularly important for climate research. However, this is not the focus of this study. Despite the limited dataset used in this study, it still provides an important preliminary geolocation assessment of AVHRR GAC dataset by indicating its geometric accuracy in different situations (e.g., satellite platform, SatZ, topography). More importantly, it identifies the threshold of SatZ under which the GAC data should be preferred in applications. To clarify our main aim of the paper, and prevent deception of readers,

we adjusted the manuscript at the following, prominent positions:

-Title: we deleted the word "global". The new title reads as follows: "*Geometric accuracy assessment of coarse resolution satellite data sets: a study based on AVHRR GAC data at the subpixel level*".

-Abstract: We clarified our main aim: "*In this study, a Correlation-based Patch Matching Method (CPMM) was proposed to characterize and quantify the geo-location accuracy at the subpixel level for satellite data with coarse resolution, such as AVHRR GAC dataset. This method is neither limited to landmarks nor suffers from errors caused by false detection due to the effect of mixed pixels caused by a coarse spatial resolution, and thus enables a more robust and comprehensive geometric assessment than existing approaches.*"

This method is expected to yield significant advantages over existing approaches in characterizing the geometric accuracy of coarse resolution dataset and enable a more comprehensive and robust geometric assessment at the sub-pixel level. We sincerely think this paper has the potential and practical values to be introduced to readers. We believe that as time goes on, the long-term AVHRR GAC data can be more comprehensively evaluated at the climate time scales.

Another major comment is related to the scientific representation, particularly the figures. What do the Y-axes of Figure 5, 6, and 7 represent? It is not clear what 0.8 (in Figure 6 (a)) or 4 (in Figure 6 (e)) meant assuming that the sum of the density of all the bins should be either 1 or 100. Please clarify the maximum value of the density.

Re: As noticed by the reviewer, it is important to understand exactly what the vertical scale is representing and how that is affected by the choice of bins when reading a histogram. If the bins are of equal size, a rectangle is erected over the bin with height proportional to the frequency—the number of cases in each bin. A histogram may also be normalized to display "relative" frequencies. In such a case, the sum of the height of all the bins should be equal to 1.

However, in the Figures 5, 6, and 7, we can see that the histograms are with non-uniform (unequal) class widths. In such a case, the area of the bin is proportional to the class frequencies, and the ordinate is labelled density instead of frequency.

$$Density = \frac{\mathrm{Re}\,lative\ frequency}{class\ \mathrm{width}}$$

Namely, it is the area of each bin that denotes the relative frequency of each class, not the height. And the total area of the histogram is equal to 1. Since the height of the bins indicate the density (not frequency), the sum of the height of all bins is unequal to 1 or 100. And the maximum value of the density is not fixed, depending on the widths of the bins. More detailed information about histograms with non-uniform width can be found at https://www.datamentor.io/r-programming/histogram/ and https://wtmaths.com/histograms_unequal_intervals.html.

In order to make the histograms more understandable to readers, we have explained the meaning of the "density" in the caption of the figure as "*For histograms, the heights of the bars indicate the density. In this case, the area of each bar is the relative frequency, and the total area of*

the histogram is equal to 1." in **Line** 310-311.

Secondly, Figures 5, 6, and 7 showed the histograms along the shifts in the along-track and across-track directions ranging from -8 and +8 kilometers with an interval, 500 meters over different study regions. Can authors show the changes in correlations along the shifts in the along-track and across-track directions as well? Here is a suggestion that authors can plot bi-histograms of 1,089 (33 x 33) samples along the shifts (the x-axis; blue for the along-track direction and red for the across-track direction) and correlations (the y-axis). Based on Figure 3, the correlations are various depending on the shifts in the directions. It might be worth showing these changes along the shifts as well. Based on these major comments, the topic and scope of this manuscript are well fit to ESSD but it is publishable after major revision.

Re: We would like to thank the reviewer here for giving such a suggestion. However, we would like to point out that the histograms in Figures 5, 6, and 7 are not derived from the 1,089 (33 x 33) simulated displacement samples. In fact, they indicate the distribution of the measured displacements of all patches within each ROI, which is used as the indicator of geometric accuracy of AVHRR GAC dataset.

As explained before, the basic idea of the method is simulating the displacements with the reference map at a step of 500 m in different directions (within the range of ±8 km), and then checking where the patch on AVHRR image and the patch on reference map match the best among the 33×33 simulated cases. The simulated displacement with the largest correlation indicates the geometric accuracy (the measured displacement) of this patch. Given that the geometric accuracy varies with SatZ, topography, etc., the image is divided into many small patches. For each patch, there are 33×33 simulated displacement samples considering different combinations of X- and Y-simulated displacements (as shown in Figure 4). The final geometric accuracy of one image was determined by statistically summarizing the measured displacements of a very large number of patches from the image (as shown in Figures 5, 6, and 7). And this is the goal of the method.

As regard to the correlations of the 33×33 simulated samples, it is their relative magnitude that is of interest, not the absolute values, as the goal is to identify the sample with the largest value among these 33×33 simulated samples. Since the reviewer is interested in the changes in correlations along the simulated shifts in the along-track and across-track directions, we presented the variations of correlations in the form of image as follows, because the images are more intuitive than bi-histogram to show the magnitude of correlation of different simulated displacements (in the four quadrants: -X,-Y, +X, +Y). Since there are so many patches for each scene (759, 632, and 469 for NOAA17, MetOp-A, and MetOp-B, respectively), it is impractical to include the results of all patches here. Thus, only part of the patches of ROI 6 on NOAA 17 scene are shown for conciseness.
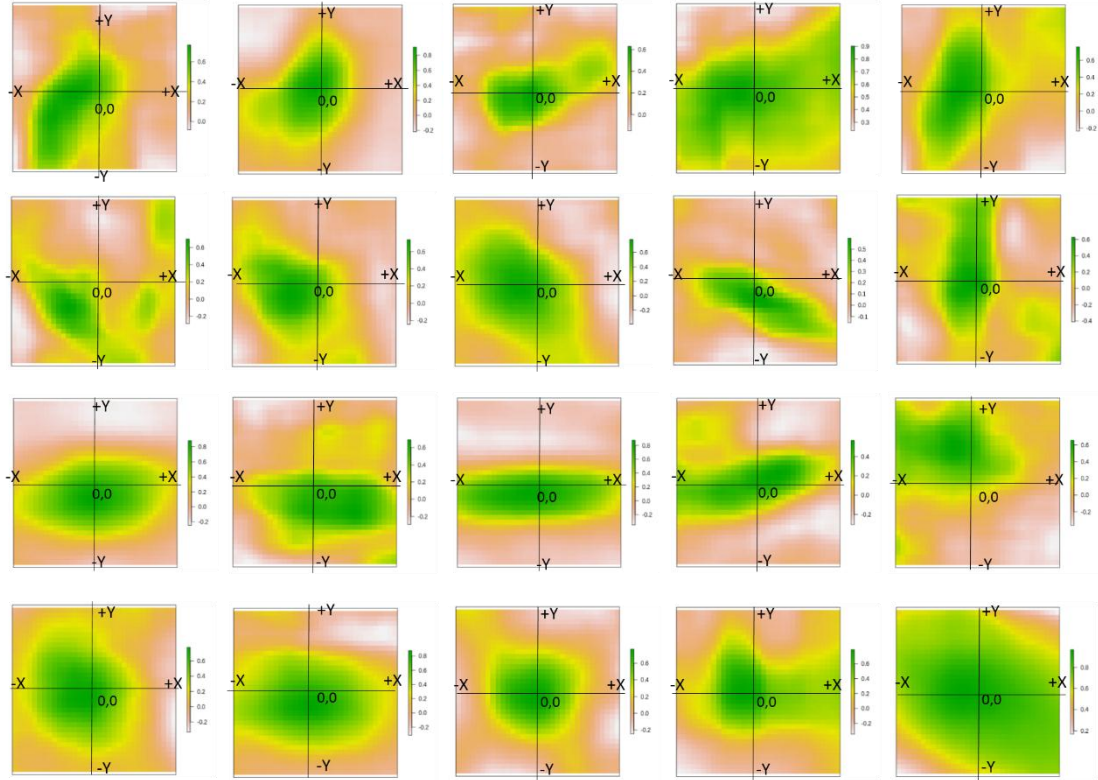
Figure. The variations in correlations of the 33×33 simulated displacements. Each subfigure represent the result of one patch. The center of the image indicates the case of no shift in two directions. Each grid represents a simulated shift combination case, which is indicated by the location of the grid away from the center in the along-track and across-track direction. The geolocation errors can be transferred into distances in kilometer (km) by multiplying the location of a grid with 500 m.

As noticed by the reviewer, the correlations are varying depending on the simulated displacements in the two directions. More importantly, the variation of correlations along the simulated shifts in the along-track and across-track directions shows very large differences from one patch to another. There is not a fixed relationship between the correlations and the simulated shifts in both directions. Actually, this is reasonable. Because when the simulated displacement is not equal to the actual geometric errors of the patch, their underlying surface is not the same. As a result, the spatial distribution spectral characteristics are not consistent between the patch on the image and that on the reference map. And the degree of their agreement (namely, the correlation) along with simulated shifts in two directions is random and differs among different patches. This can also be confirmed by the above figure.

In fact, the changes in correlations are related to the proximity of the simulated displacement to the actual displacement of the patch (taken from AVHRR GAC scene). From the above figure, it can be seen that the correlation appears a maximum at a certain location, and then becomes gradually smaller with increasing distance from that location. The location with the maximum correlation indicates the actual displacement of this patch. The farther away the simulated displacement are from that location, the smaller the correlations.

In conclusion, the change in correlations do not show a clear trend along the simulated shifts in the along-track and across-track directions. Instead, the correlations show a decreasing trend with the distance deviated from the location corresponding to the actual geometric error of the patch (AVHRR GAC). In order to clarify this point, we have added one sentence as "*It can be seen that the correlation appears a maximum at a certain location, and then becomes gradually smaller with increasing distance from that location. The location with the maximum correlation indicates the actual displacement of this patch.*" in **Line** 261-263 in the new manuscript.

Minor comments are provided below:

Line 9: Global Area Coverage (GAC), not GAC (Global Area Coverage).

Re: "GAC (Global Area Coverage)" has been changed to "*Global Area Coverage (GAC)*".

Line 34: "are" instead of "is"

Re: This error has been corrected.

Line 61: What does "reduced resolution" mean here? Maybe "coarse resolution"?

Re: Local Area Coverage (LAC) data has a spatial resolution of 1.1 km. Global Area Coverage (GAC) data has a spatial resolution of 4 km. Here, "*reduced resolution*" means lower spatial resolution. In order to make it clearer to readers, we have changed it to "*coarser resolution*" in the new manuscript.

Line 81: What are "certain conditions"? Please explain it in more details.

Re: We agree, the term "certain conditions" is not clearly defined and the explanation followed in the subsequent sentences wasn't clear enough linked. We thus re-phrased this section in **Line** 82-90 as follows:

"*The abilities of these three methods in characterizing the geometric errors are limited and dependent on different, method-dependent factors. Whereas, the CCM is subject to the structure of coastline, and the LFM depends on the accuracy of the land-sea model but shows advantages on complex coastlines (Han et al., 2016). The coregistration method is usually applied to high-resolution visible and infrared images (Wang et al., 2013; Wolfe et al., 2013) as it relies on individual objects/landmarks in both datasets. However, when it comes to coarse resolution data with several kilometers' pixel size, the main difficulties arise from false detection due to the effect of mixed pixels, which hampers the application of the existing methods. An approach assessing the geolocation accuracy of coarse resolution satellite data is thus strongly needed.*"

Line 82-83: "... but *it* depends on ..." Also, is this sentence based on previous studies? If then, please cite the reference.

Re: This sentence has been rephrased as "*......, and the LFM depends on the accuracy of the land-sea model but shows advantages on complex coastlines (Han et al., 2016)*" in **Line** 84-85. This sentence is based on a previous study, which has been cited in the new manuscript.

Line 100-101: The sentence is not clear. Maybe "to test some satellite data from NOAA-17, ..."

Re: This sentence has been rephrased as "*This method is tested using satellite data from NOAA-17, MetOp-A, and MetOp-B, respectively.*" in **Line** 105-106.

Line 165-166: Please consider to change the ROI numbers. For example, for the mountainous areas, the ROI numbers are 1, 2, and 3 (currently, 2, 4, and 6, respectively). For the flat regions, the ROI numbers are 4, 5, and 6 (currently, 1, 3, and 5).

Re: We would like to thank the reviewer here for giving such a suggestion. As pointed out by the manuscript, the ROIs are distributed over different latitudes and longitudes, different geographic locations, different SatZ angles, different land covers, as well as different topographies in order to explore the potential impact factors related to geolocation accuracy. The topography is only one of factors that need to be considered. Therefore, the ROIs are not numbered in the order in which only mountainous/flat regions are considered. In fact, the number of the ROI is just used as a label, and we would like to keep the ROI numbers in Figure 1 in the new manuscript.

Figure 2: Please use different ROI labels since they are different from regions of interest in Figure 1. It is confusing if the numbers are used for ROI labels in Figure 1 and Figure 2. I suggest authors to use letters for ROI indicators (e.i., A, B, C, D, E, and F) in Figure 2.

Re: As suggested by the reviewer, we have used letters (i.e., a, b, c, d, e, and f) for ROI indicators in Figure 2.

Line 187: "CCM", not "CGM".

Re: "CGM" has been revised as "CCM"

Line 187: land-sea fraction method (LFM) since the full name of LFM appeared in line 76.

Re: This has been corrected.

Line 187-191: These sentences are redundant. Please remove them.

Re: This sentence has been removed in the new submission.

Figure 3: Please use white filled boxes or arrows, instead of blue filled boxes or arrows.

Re: We have used white filled boxes or arrows in the figure.

Line 218-219: I have a major concern about the robustness of this method for other regions and other seasons. Please see my first major concern above.

Re: As explained above, the method itself is based on correlation calculation between the patches taken from AVHRR GAC image and the patches with simulated displacement taken from the reference map. The geometric error of one patch was indicated by the simulated displacement with the largest correlation. And the final geometric accuracy was determined by statistically summarizing the measured displacements of a very large number of patches (759, 632, and 469 for NOAA17, MetOp-A, and MetOp-B, respectively) from the image.

There are four basic requirements of the method:

First, the reference image should have much higher spatial resolution than the image that is to be evaluated (e.g., 500m vs. 4 km in this study).

Second, referenced image itself should have high geometric accuracy.

Third, with consideration of temporal variations of the spectral properties of the Earth surface, the date of the reference image should be equal or close to the image to be evaluated.

Last but not the least, the individual patches should present a spatially heterogeneous distribution of surface characteristic and thus varying spectra. Homogeneous surface (e.g., water, desert) should be avoided, as for these surfaces, the correlations are always large and similar in any simulated displacement cases. Consequently, it is hard to identify the actual displacement of the patch on the AVHRR GAC image.

It is obvious that the method works directly on pixel values. It is thus neither dependent on regions nor on seasons. As long as the reference image and the ROI satisfy the above requirements, the method can be applied to other regions and seasons. In order to clarify this point, we added one sentence as "*Although this assessment was only conducted for a single scene of each satellite, the highly variable ROIs take the influential factors of geometric accuracy well into account. Therefore, the presented conclusions are transferable to other regions or seasons. However, it is noteworthy that this method is not applicable to homogeneous surface (e.g., water, desert), where the correlations are almost the same in any simulated displacement cases.*" in **Line** 569-573.

Figure 4: Please use a larger range of the color scale. It is hard to find the grid cell/location of the maximum correlation.

Re: The color scale has been optimized by algorithmic procedures, and only the minimum and maximum were covered. The difficulty to find the maximum correlation in Figure 4 lies in the fact that the correlations of simulated displacements which are close to the actual displacement of one patch are similar and approach the maximum correlation. But this will not affect the final results because the maximum correlation is identified through the algorithm, not from the image in the figure. The Figure 4 just shows an example of one patch for illustration purposes. The main aim of Figure 4 is to help readers better understand the process of determining the displacement of one patch.

Line 275-277: Mean and standard deviation are parametric statistics of the data that are from a normal distribution. However, the shifts might be not well fitted to a normal distribution (based on Figure 3). I suggest authors to use the median of the shifts and their first and third quartiles.

Re: We would like to thank the reviewer here for your valuable advice. According to Han et al. (2016), Sultan et al. (2015), Aguilar et al. (2013), and Bicheron et al. (2011), geometric accuracies are generally measured as the mean shifts and standard deviations, with the former representing the magnitude of the displacements and the latter indicating the uncertainty. The small standard deviation values indicate a high reliability for the geometric accuracy assessment. In line with previous studies, the mean and standard deviation were adopted in this study.

Since the reviewer is interested in the result with the median of the shifts and their first and third quartiles, the boxplots of the displacements in the across-track and along-track directions are presented here.
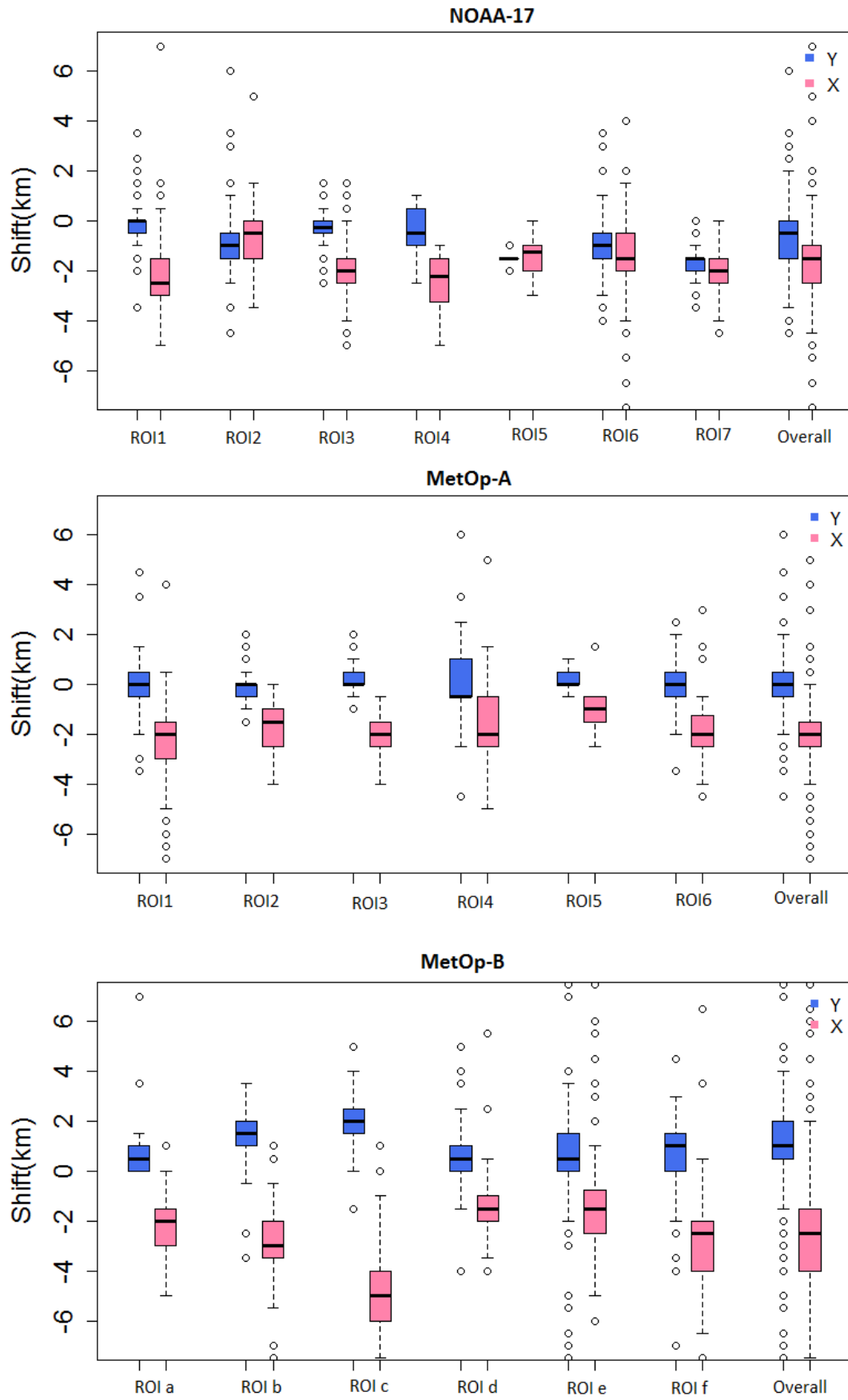
Figure. The boxplots of shifts in the across-track (X) and along-track (Y) directions over different

regions for NOAA-17, MetOp-A, and MetOp-B scenes.

From the above figure, it can be seen that the scenes from these satellites all present West shifts in the across-track direction. In regard to the shifts in the along-track direction, NOAA-17 generally shows South shifts. By contrast, the MetOp-B mainly present North shifts. And the MetOp-A scene shows a distinct advantage over NOAA-17 and MetOp-B in the along-track direction without obvious shifts. The geolocation accuracy in the along-track direction is always higher and with less uncertainties than the across-track direction given their closeness to 0 and more centralized distribution.

In fact, the conclusions based on the boxplots are consistent with those based on the histograms with mean and standard deviations shown in the manuscript. Moreover, the histograms are more straightforward to show the distribution of displacements at different levels. For these reasons, we would like to keep the mean and standard deviation (as well as the histograms) as the indicators of geometric accuracy in the new manuscript.

Reference:

Aguilar, M. A., Salda?a, Mar á del Mar, & Aguilar, F. J. . (2013). Assessing geometric accuracy of the orthorectification process from geoeye-1 and worldview-2 panchromatic images. International Journal of Applied Earth Observation and Geoinformation, 21, 427-435.

Bicheron, P. , Amberg, V. , Bourg, L. , Petit, D. , & Arino, O. . (2011). Geolocation assessment of meris globcover orthorectified products. IEEE Transactions on Geoscience and Remote Sensing, 49(8), 2972-2982.

Han, Y. , Weng, F. , Zou, X. , Yang, H. , & Scott, D. . (2016). Characterization of geolocation accuracy of suomi npp advanced technology microwave sounder measurements. Journal of Geophysical Research: Atmospheres, 121(9), 4933-4950.

Sultan, Aksakal , et al. "Geometric Quality Analysis of AVHRR Orthoimages." Remote Sensing 7.3(2015):3293-3319.

Line 282-283: Please rewrite this sentence in the order of ROIs 5 and 6.

Re: Here, the ROIs are sorted in ascending order according to the magnitude of displacements. Since the ROI6 has a smaller shifts of -1.33 than that of ROI5 (-1.35), the ROI6 rank in the front of ROI5.

Line 284 and 286: "ROIs *1, 3, 4, and 7*" Is there any reason to keep the order of ROIs (7, 3, 1, 4)?

Re: As explained above, the order of these ROIs agrees with the order of the magnitude of their displacements.

Line 291: "ROIs 2, *5, and 6*"

Re: This order agrees with the order of the magnitude of their shifts.

Figure 5: Please state what the blue and red histograms represent.

Re: We would like to thank the reviewer for this valuable advice. In order to make the figure more easy to read, we have explained the blue and red histograms in the caption of the figure as

"*Figure 5. The distribution of shifts in the across-track (X, represented by red histogram) and along-track (Y, denoted as blue histogram) directions over different regions for NOAA-17 scene. The unit of the shift is km.*".

Table 2, 3, and 4: Please add the elevations of ROIs. This information will be helpful for readers to understand the impact of elevation on the accuracy.

Re: As suggested by the reviewer, the elevation information of these ROIs was extracted from SRTM Digital Elevation Data Version 4 as following. It can be seen that the elevations are widely distributed for each ROI. Therefore, the averaged elevations for each ROI were calculated and added in Table 2, 3 and 4.
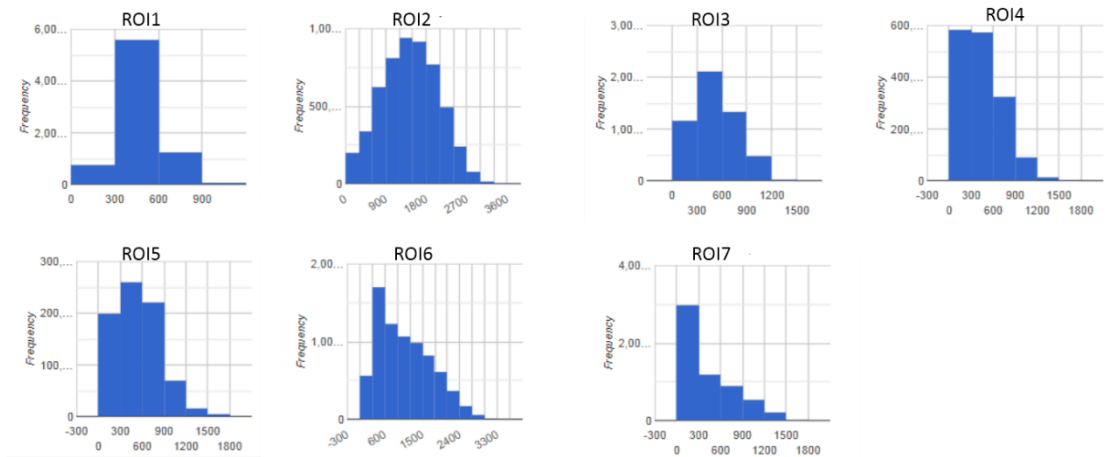
Figure. The histograms of elevations within these ROIs for the scenes from NOAA-17 and MetOp-A.
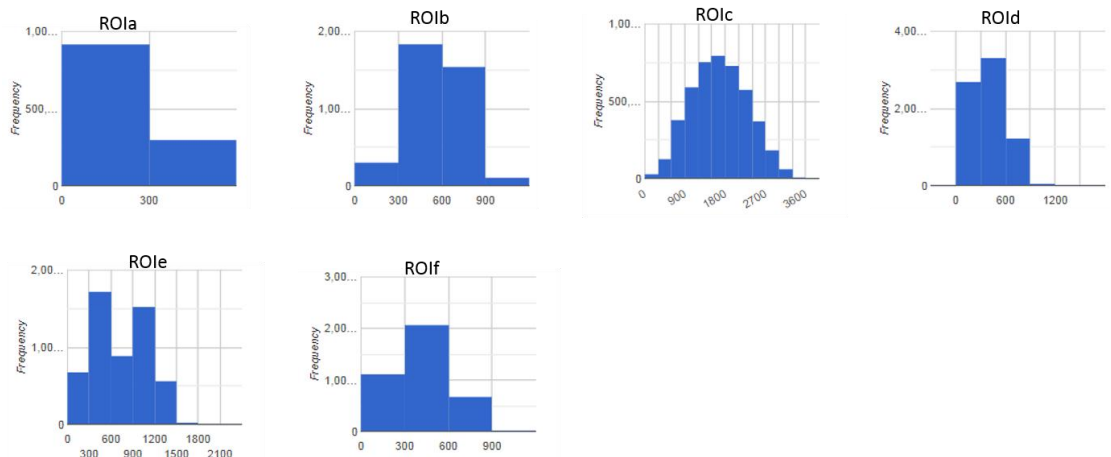
Figure. The histograms of elevations within these ROIs for the scenes from MetOp-B.

Figure 8: "SatZ (*a-f*), longitude (*g-i*), and latitude (*j-l*)"

Re: We have corrected this mistake in the new manuscript. The caption of Figure 8 has been revised as "*Figure 8. Influence of SatZ on the geolocation accuracy in the across-track (a-c) and along-track (d-f) directions. (g-i) and (j-l) describe the influence of longitude and latitude on the geolocation accuracy in the across-track and along-track directions, respectively. The left column*

indicates results of NOAA-17 (blue), middle for MetOp-A (red), and right for MetOp-B (pink) scenes.".

Line 495-496: Please remove this sentence.

Re: This sentence has been removed as suggested by the reviewer.

Line 499: "... within the range *between* -8 ∘ *and* 0 ∘ *(Fig. 8 h and i, respectively)*".

Re: This sentence has been rephrased as "*…… and neither does MetOp-B within the range between -8 ° and 0 ° (Fig. 8 h and i, respectively)*" in **Line** 509-510 in the new manuscript as suggested by the reviewer.

Line 558-559: As authors mentioned, this study was conducted only for a single scene. It questions: 1) is this study novel enough to contribute to various applications of the satellite data used in this study (particularly for climate research)? Or, was conducted a comprehensive assessment for the robustness of this method. The current results are more likely based on a case study for geometric accuracy assessment of coarse resolution satellite datasets.

Re: We admit that the current results are based on a case study for geometric accuracy assessment of coarse resolution satellite datasets. We now clearly state this in the revised Title and Abstract, please see our answer above. As mentioned earlier, a comprehensive geometric assessment of AVHRR GAC dataset over a long time series was not the focus of this study. Instead, this study aims to propose a geometric assessment method specified for coarse resolution satellite datasets. However, we insist on that the method is novel to support a comprehensive geometric assessment for various applications and that the assessment of this method is comprehensive in this study. This can be explained from following aspects:

1. The traditional methods do not work well with coarse resolution dataset due to the fact that the detection of any robust feature fails. Even for the relatively stable lake and sea shorelines, errors may be introduced due to the false detection resulted from the effect of mixed pixels. Furthermore, such evaluations are often limited to certain landmarks, which cannot represent the overall performance of one scene. Because the geometric accuracy varies with satellite zenith angle, latitudes and longitudes, and topography, etc. As a result, the geometric accuracy of AVHRR GAC dataset has not yet been adequately addressed, particularly over terrain areas. Since the commonly used methods are difficult to apply on coarse resolution imagery, this study has brought forward a way of thinking in another view, namely simulating the displacements with the reference map at a certain step length in different directions, and then checking where the image and the reference map match the best, the Correlation-based Patch Matching Method (CPMM). The basic principle is that when the simulated displacements is equal to the geometric errors of the coarse-resolution image, the correlation between image and reference map is the largest given that the spatial distribution characteristics of their spectrums are completely consistent. Since this method works directly on pixel values, it does not suffer from errors caused by false detection due to the effect of mixed pixels and is not limited to a certain landmark. Therefore, it enables a more accurate and more

comprehensive geometric assessment. Moreover, it provides the opportunity to explore the influential factors on geometric accuracy. This method is expected to yield significant advantages over existing approaches and enables achieving a subpixel geo-positioning accuracy of coarse resolution datasets.

2. Despite that only single scene was used in this study, the ROIs are of great variety covering different latitudes and longitudes, SatZ angles, land covers, as well as varying topographies, which represent the several typical influential factors on geometric accuracy. Furthermore, the surface condition of these ROIs is very complicated, which is similar to most of the land surfaces on earth (apart from homogeneous regions such as water and desert). Moreover, it is important to remember that the method is not dependent on regions or seasons as long as the reference image and the ROI satisfy the above-mentioned requirements. Therefore, it is reasonable to believe that the assessment of this method is comprehensive and robust.

3. As for the contributions to various applications of the AVHRR GAC data (particularly for climate research), we admit that the limited dataset does not provide a comprehensive geometric assessment of the AVHRR GAC dataset over the entire time span that the dataset is available. However, the method itself supports the geometric assessment in the long time series because it is independent of regions and seasons and could thus be applied to other NOAA sensors providing AVHRR GAC data. Given that there are so many factors influencing geometric accuracy (e.g., satellite platform, orbital drift, SatZ, terrain, latitude), the AVHRR GAC data should be evaluated for all NOAA and MetOp platforms throughout the lifetime of the dataset globally, which is particularly important for climate research. Therefore, a comprehensive time series analysis of the geometric accuracy of AVHRR GAC data is needed in the future. This study, however, still provides an important preliminary geolocation assessment by indicating the displacement of AVHRR GAC data in different situations (e.g., satellite platform, SatZ, topography).

Response to Referee #2

Thank you for spending your time on my manuscript and giving the opportunity to revise it. And we also thank you for your valuable comments as they actually improve the paper's quality. In this document, we describe how we address the reviewer's comments. The reviewer's comments are marked in black color, however, our reply is marked in blue color.

This paper describes the work undertaken by the authors to assess the geolocation accuracy at the subpixel level of AVHRR Global Area Coverage data from NOAA-17, MetOp-A and MetOp-B satellites. The paper is comprehensive and generally well written, with sufficient figures to follow the work that is described. The authors used a coregistration method based on reference NDVI data from MODIS. The authors use NDVI from NOAA-17, MetOp-A and MetOp-B satellites (using visible and near IR bands), and use the described Correlation-based Patch Matching Method to assess the sub-pixel geo-location accuracy in both the along-track and cross-track directions. Six regions of interest from Europe and Africa were selected for analysis, and included different land cover and terrain characteristics. The effect of large satellite zenith angles was also examined. Results are presented as mean cross-track and along-track shifts along with a standard deviation for each of the satellites applied to each of the regions of interest. The analysis was thorough, and I cannot suggest any further work needed for the paper.

I have a few specific comments for the paper:

1) Provide a reference or two on the land-sea fraction method mentioned on page 3.

Re: A reference (i.e. Bennartz, 1999) has been provided for land-sea fraction method in **Line** 85.

2) When introducing figures 1 and 2, point out the color bar for SatZ and that the white line represents small SatZ along the satellite path. This will be helpful to the reader.

Re: We have pointed out the meaning of color bar and the white line in the captions of figures 1 and 2 in the new manuscript. The caption of figure 1 was revised as "***Figure 1.******…….*** *(b) and (d) are their corresponding SatZ respectively, which is indicated by the color bar, with the white line representing small SatZ along the satellite path.*" in **Line** 182-183. And the caption of figure 2 was revised as "***Figure 2.******…….****(b) and (d) are their corresponding SatZ (indicated by the color bar), respectively. The white line in (d) represents small SatZ along the satellite path.*" in **Line** 186-187.

3) The figure 8 caption is not cor- rect. The first two rows are SatZ cross-track and along-track (a-c) and (d-f). Longitude should be (g-i). Latitude should be (j-l).

Re: We have corrected this mistake in the new manuscript. The caption of figure 8 has been revised as "***Figure 8****. Influence of SatZ on the geolocation accuracy in the across-track (a-c) and along-track (d-f) directions. (g-i) and (j-l) describe the influence of longitude and latitude on the geolocation accuracy in the across-track and along-track directions, respectively. The left column indicates results of NOAA-17 (blue), middle for MetOp-A (red), and right for MetOp-B (pink) scenes.*".

Geometric accuracy assessment **of coarse resolution satellite data sets**: a study based on AVHRR GAC data at the subpixel level

Xiaodan Wu[1, 2], Kathrin Naegeli[2], and Stefan Wunderle[2]

[1]College of Earth and Environmental Sciences, Lanzhou University, Lanzhou 730000, China

[2]Institute of Geography and Oeschger Center for Climate Change Research, University of Bern, Hallerstrasse 12, CH-3012 Bern, Switzerland

Correspondence to: Xiaodan Wu (wuxd@lzu.edu.cn)

Abstract: AVHRR Global Area Coverage (GAC) data provide daily global coverage of the Earth, which are widely used for global environmental and climate studies. However, their geolocation accuracy has not been comprehensively evaluated due to the difficulty caused by onboard resampling and the resulting coarse resolution, which hampers their usefulness in various applications. In this study, a Correlation-based Patch Matching Method (CPMM) was proposed to characterize and quantify the geo-location accuracy at the subpixel level for satellite data with coarse resolution, such as AVHRR GAC dataset. This method is neither limited to landmarks nor suffers from errors caused by false detection due to the effect of mixed pixels caused by a coarse spatial resolution, and thus enables a more robust and comprehensive geometric assessment than existing approaches. Data of NOAA-17, MetOp-A, and MetOp-B satellites were selected to test the geocoding accuracy. The three satellites predominately present West shifts in the across-track direction, with average values of -1.69 km, -1.9 km, -2.56 km and standard deviations of 1.32 km, 1.1 km, 2.19 km for NOAA-17, MetOp-A, and MetOp-B, respectively. The large shifts and uncertainties are partly induced by the larger satellite zenith angles (SatZ) and partly due to the terrain effect, which is related to SatZ and becomes apparent in the case of large SatZ. It is thus suggested that GAC data with SatZ less than 40° should be preferred in applications. The along-track geolocation accuracy is clearly improved compared to the across-track direction, with average shifts of -0.7 km, -0.02 km, 0.96 km and standard deviations of 1.01 km, 0.79 km, 1.70 km for NOAA-17, MetOp-A, and MetOp-B, respectively. The data can be accessed from http://www.esa-cloud-cci.org/ (Stengel et al., 2017) and https://ladsweb.modaps.eosdis.nasa.gov/ (Didan, 2015).

1 Introduction

Advanced Very High Resolution Radiometer (AVHRR) data provide valuable data sources with a near daily global coverage to support a broad range of environmental monitoring researches, including weather forecasting, climate change, ocean dynamics, atmospheric

34   soundings, land cover monitoring, search and rescue, forest fire detection, and many other

35   applications (Van et al., 2008). The unique advantage of AVHRR sensors is their long history

36   dating back to the 1980s and thus enabling long-term analyses at climate-relevant time scales

37   that cannot be covered by other satellites. However, AVHRR data are rarely used at the full

38   spatial resolution for global monitoring due to the limited data availability (Pouliot et al., 2009;

39   Fontana et al., 2009). Instead, the Global Area Coverage (GAC) AVHRR dataset with a reduced

40   spatial resolution is generally employed in long-term studies at a global or regional perspective

41   (Hori et al., 2017; Delbart et al., 2006; Stöckli et al., 2004; Moulin et al., 1997).

42   However, there are several known problems with the geo-location of AVHRR GAC data,

43   which have a profound impact on their application. (1) The drift of the spacecraft clock results

44   in errors in the along-track direction (Devasthale et al., 2016). Generally, an uncertainty of 1

45   second approximately induces an error of 8 km in this direction. (2) Satellite orientation and

46   position uncertainties influence the projection of the satellite geometry to the ground, which

47   leads to errors in both along-track and across-track directions. (3) Earth surface elevation

48   aggravates distortions in the across-track direction (Fontana et al., 2009). Without navigation

49   corrections, the spatial misplacement of the GAC scene caused by these factors can be up to

50   25-30 km occasionally (Devasthale et al., 2016).

51   For geocoding of AVHRR data, a two-step approach is usually used: 1) geocoding based

52   on orbit model, ephemeris data, and time of onboard clock (Van et al., 2008), achieving an

53   accuracy within 3-5 km depending on the accuracy of orbit parameters and model (Khlopenkov

54   et al., 2010); 2) using any kind of ground control points (GCPs) (e.g., road or river intersections,

55   coastal lines) to improve geocoding (Takagi, 2004; Van et al., 2008). Additionally, in order to

56   eliminate the ortho-shift caused by elevations, an orthorectification would be needed (Aguilar

57   et al., 2013; Khlopenkov et al., 2010). The dataset used in this study is from the ESA (European

58   Space Agency) cloud CCI (Cloud Climate Change Initiative) project, which has corrected clock

59   drift errors by coregistration of AVHRR GAC data with a reference dataset, and showed

60   improved navigation by fitting the data to coastal lines.

61   Unlike the Local Area Coverage (LAC) data with a full spatial resolution of AVHRR, GAC

62   data are sampled on board the satellite in real-time to generate coarser resolution data (Kidwell,

63   1998). This is achieved by averaging values from four out of five pixel samples along a scan

64   line and eliminating two out of three scan lines, resulting in a spatial resolution of 1.1 km × 4

65   km along the scan line with a 3 km distance between pixels across the scan line. Therefore, the

66   nominal size of a GAC pixel is 3 km × 4.4 km. It is important to note that the spatial resolution

67   of GAC data also depends on the satellite zenith angle (SatZ). Because of the large swath width,

68   the spatial resolution of LAC decreases to 2.4km by 6.9 km at the edge of the swath (D'Souza

69   et al., 1994). With the selection process for GAC, the GAC resolution is also much worse than

70   4 km. Furthermore, the onboard resampling process of GAC data makes the orthorectification

71   not feasible, which results in lowering of geolocation accuracy in the across-track direction.

72   The final quality of AVHRR GAC data has not been quantified and we, therefore, make an

73   attempt to assess their geolocation accuracy, particularly over terrain areas.

74   There are generally three approaches to assess the non-systematic geometric errors of

75 satellite images: (1) the coastline crossing method (CCM) which detects the coastline in the

76 along-track and across-track directions through a cubic polynomial fitting (Hoffman et al.,

77 1987); (2) the land-sea fraction method (LFM) which develops a linear radiance model as a

78 function of land-sea fraction, land and sea radiance, and then finds the minimum difference

79 between model-simulated and instrument-observed radiance by shifting the pixels in along-

80 track and across-track directions (Bennartz, 1999); (3) the coregistration method which

81 computes the difference or similarity relative to a reference image (Khlopenkov et al., 2010).

82 The abilities of these three methods in characterizing the geometric errors are limited and

83 dependent on different, method-dependent factors. Whereas, the CCM is subject to the structure

84 of coastline, and the LFM depends on the accuracy of the land-sea model but shows advantages

85 on complex coastlines (Han et al., 2016). The coregistration method is usually applied to high-

86 resolution visible and infrared images (Wang et al., 2013; Wolfe et al., 2013) as it relies on

87 individual objects/landmarks in both datasets. However, when it comes to coarse resolution

88 data with several kilometers' pixel size, the main difficulties arise from false detection due to

89 the effect of mixed pixels, which hampers the application of the existing methods. An approach

90 assessing the geolocation accuracy of coarse resolution satellite data is thus strongly needed.

91 The geometric accuracy is important as even small geometric errors can lead to significant

92 noises on the retrieval of surface parameters, such as NDVI, LAI, and albedo, which mask the

93 reality or bias the final results and conclusions (Khlopenkov et al., 2010; Arnold et al., 2010).

94 For instance, anomalous NDVI dynamics during the regeneration phase of forest fire-burnt

95 areas can be explained by the imprecise geolocation of the data set used (Alcaraz-Segura et al.,

96 2010). Therefore, it is critical to develop a rigorous geometric accuracy assessment method in

97 order to ensure the effectiveness of AVHRR GAC data in the generation of climate data records

98 (CDR) (Khlopenkov et al., 2010; Van et al., 2008).

99   Based on the idea of the coregistration method, this study proposes a method named

100 Correlation-based Patch Matching Method (CPMM), which is capable of quantifying the

101 geometric accuracy of coarse resolution satellite data available as fundamental climate data

102 records (FCDR) for global applications (Hollmann et al., 2013). We show the procedure based

103 on AVHRR GAC data, which are compiled for the ESA CCI cloud project (Stengel et al., 2017)

104 and are now also used for the ESA CCI+ snow project. The assessment is conducted at the sub-

105 pixel level and not affected by the mixed pixel problem. This method is tested using satellite

106 data from NOAA-17, MetOp-A, and MetOp-B, respectively. Furthermore, the potential factors

107 that cause geometric distortions are explored and discussed. Although the band-to-band

108 registration (BBR) accuracy assessment is an important aspect for such multi-spectral images,

109 it is not a focus of this study, since the BBR accuracy of AVHRR has been comprehensively

110 evaluated by a previous study (Aksakal et al., 2015).

2 Data and geographical regions of interest

2.1 Satellite data

AVHRR is a multipurpose imaging instrument aboard on the NOAA satellite series since 1978 and the Meteorological Operational Satellites (MetOp) operated by EUMETSAT since 2006, delivering daily information of the Earth in the visible, near-infrared, and thermal wavelengths. They provide observations from 4 to 6 spectral bands, depending on the generation of AVHRR sensors. This study only focuses on the AVHRR GAC data observed by NOAA-17 (AVHRR-3 generation), MetOp-A, and MetOp-B. The spectral characteristics of the AVHRR sensors on board these three platforms are the same and summarized in Table 1. Since the spatial resolution of AVHRR GAC data is often considered to be 4 km (Fontana et al., 2009), the analysis in this study was conducted at the 4 km level using the data acquired on August 13, 2003 for NOAA-17 and March 12, 2017 for MetOp-A and MetOp-B.

Table 1. Spectral characteristics of AVHRR sensors

Band	Wavelength (μm)	Application
1	0.58–0.68 (VIS)	Cloud mapping, vegetation and surface characterization
2	0.72–1.00 (NIR)	Vegetation mapping, water body detection
3a*	1.58–1.64 (MIR)	Snow and Ice classification
3b*	3.55–3.93 (MIR)	Cloud detection, Sea/Land surface temperature,
4	10.30–11.30 (TIR)	Cloud detection, Sea/Land surface temperature,
5	11.50–12.50 (TIR)	Cloud detection, Sea/Land surface temperature

*Note: Channel 3a is only used continuously on NOAA-17 and MetOp-A. On-board MetOp-B channel 3a was only active during a limited time span.

From a standpoint of geometric accuracy assessment, the reflectances in band 1 and 2 were employed in this study. However, these two bands are not only affected by the atmosphere but also by the earth surface anisotropy characterized by the bidirectional reflectance distribution function (BRDF) (Cihlar et al., 2004). Given the fact that BRDF effects can be reduced through the calculation of vegetation indices such as NDVI (Lee & Kaufman, 1986), the NDVI is employed in this study, which is derived from the reflectance in band 1 and 2 according to Equation (1).

$$NDVI = \frac{R_2 - R_1}{R_2 + R_1} \tag{1}$$

where R_1 and R_2 refer to the reflectance in band 1 and 2, respectively. It is important to note that during the process of generating NDVI, the atmospheric and BRDF corrections were not performed. But it is expected that such effects originating from these omissions are of minor influence, because the method of this study is based on correlation analysis and does not rely

138 on absolute values of NDVI. Another advantage of using NDVI is that it has higher contrast

139 between different land cover types, such as vegetation/no-vegetation, snow/no-snow, etc.

140 Furthermore, in order to investigate the effect of off-nadir viewing angle on geometric accuracy,

141 the SatZ data of AVHRR were also extracted.

142 Ideally, the referenced data in geometric quality assessment should meet the required

143 accuracy of 1/3 field of view (FOV) (WMO and UNEP, 2006), and also satisfy the accuracy

144 requirement of an order of magnitude better than one-tenth of the image spatial resolution

145 (Aksakal, 2013), which means 400 m for the AVHRR GAC data. The NDVI provided by

146 MOD13A1 V006 product was introduced as a source of reference data to perform the geometric

147 quality assessment, because the sub-pixel accuracy of MODIS product is sufficient to satisfy

148 this requirement (Wolfe et al., 2002). The high geolocation accuracy of MODIS products was

149 achieved by using the most advanced data processing system, which has updated the models of

150 spacecraft and instrument orientation several times since launch. Consequently, the various

151 geolocation biases resulted from instrument effects and sensor orientation are removed (Wolfe

152 et al., 2002). The NDVI data with the date corresponding to that of AVHRR GAC data, were

153 obtained from the Level-1 and Atmosphere Archive & Distribution System (LAADS)

154 Distributed Active Archive Center (DAAC) (https://ladsweb.modaps.eosdis.nasa.gov/) with

155 the sinusoidal projection at a spatial resolution of 500 m and a temporal resolution of 16-day.

156 The detailed description of the MOD13A1 V006 product can be found in Didan (2015).

157 **2.2 Geographical regions of interest**

158 The purpose of this study is not only to assess the geolocation accuracy of 4 km AVHRR

159 GAC data, but also to explore the potential impact factors related to geolocation accuracy.

160 Therefore, the investigations were made at different latitudes and longitudes, at different

161 locations with different SatZ, for different land covers, as well as different topographies. The

162 swaths covering parts of Europe (including the alpine mountain) and Africa were used since

163 they fit the study needs (Fig. 1). Investigations were based on six regions of interest (ROI) as

164 shown in Figs. 1 and 2. The ROIs from 1 to 6 enable us to investigate the geolocation accuracy

165 at different SatZ, topography, as well as latitudes and longitudes. Their locations and extents

166 are consistent for the scenes from NOAA-17 and MetOp-A (Fig. 1), which enables the

167 comparison of geolocation accuracy between these two sensors. The size of ROI was attempted

168 to be set as large as possible in order to get more significant and comprehensive results. On the

169 other hand, areas covered by cloud and water have to be avoided, resulting in the different sizes

170 of these ROIs. Half of the ROIs (ROIs 2, 4, 6) serve as a good example for a typical

171 mountainous areas on Earth. The other half of ROIs (ROIs 1, 3, 5), on the other hand, mainly

172 cover relatively flat areas. Since the NOAA-17 scene was almost unaffected by cloud, another

173 ROI (ROI 7) was selected to check the geolocation accuracy at nadir. The MetOp-B scene was

174 influenced by cloud but served as a good example to illustrate the combined effect of

175 topography and large SatZ (Fig. 2). Although there are also 6 ROIs (ROIs (a-f)) selected, their

sizes and extents are totally different from the above two scenes. In order to include the terrain area, two subsets were used (Figs. 2a and c). Each grid in the ROI represents the minimum unit (namely the patch) based on which we conduct the geometric quality analysis.
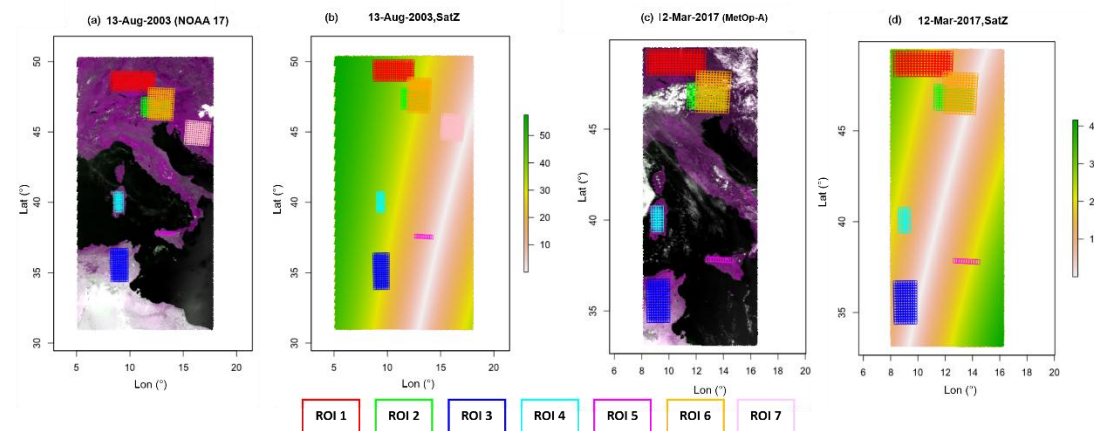

Figure 1. The study area and the distribution of ROIs. (a) and (c) are the composite maps of bands 2-1-1 of AVHRR GAC data on August 13, 2003 and March 12, 2017, respectively. (b) and (d) are their corresponding SatZ respectively, which is indicated by the color bar, with the white line representing small SatZ along the satellite path.
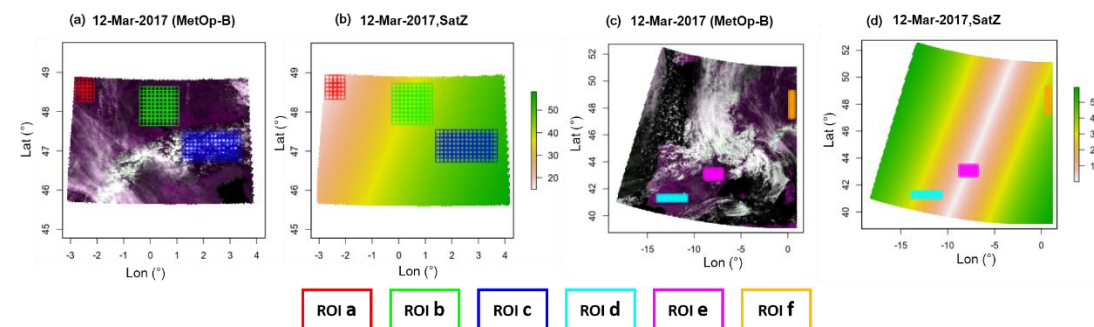

Figure 2. The study area and the distribution of ROIs on March 12, 2017. (a) and (c) are the composite maps of bands 2-1-1 subset 1 and 2, respectively. (b) and (d) are their corresponding SatZ (indicated by the color bar), respectively. The white line in (d) represents small SatZ along the satellite path.

3 Methodology

The assessment was performed by comparing the AVHRR GAC scenes with geo-located reference data, i.e. MOD13A1 (V006). An approach named Correlation-based Patch Matching Method (CPMM) is proposed to find the best match between small image patches taken from the reference images and the AVHRR GAC images. This method is expected to be more suitable for the geometric accuracy assessment of coarse resolution images than the current methods, i.e. the CCM, LFM, and co-registration using shorelines. The framework of CPMM is shown in Fig. 3, and the detailed description of this method is provided below.
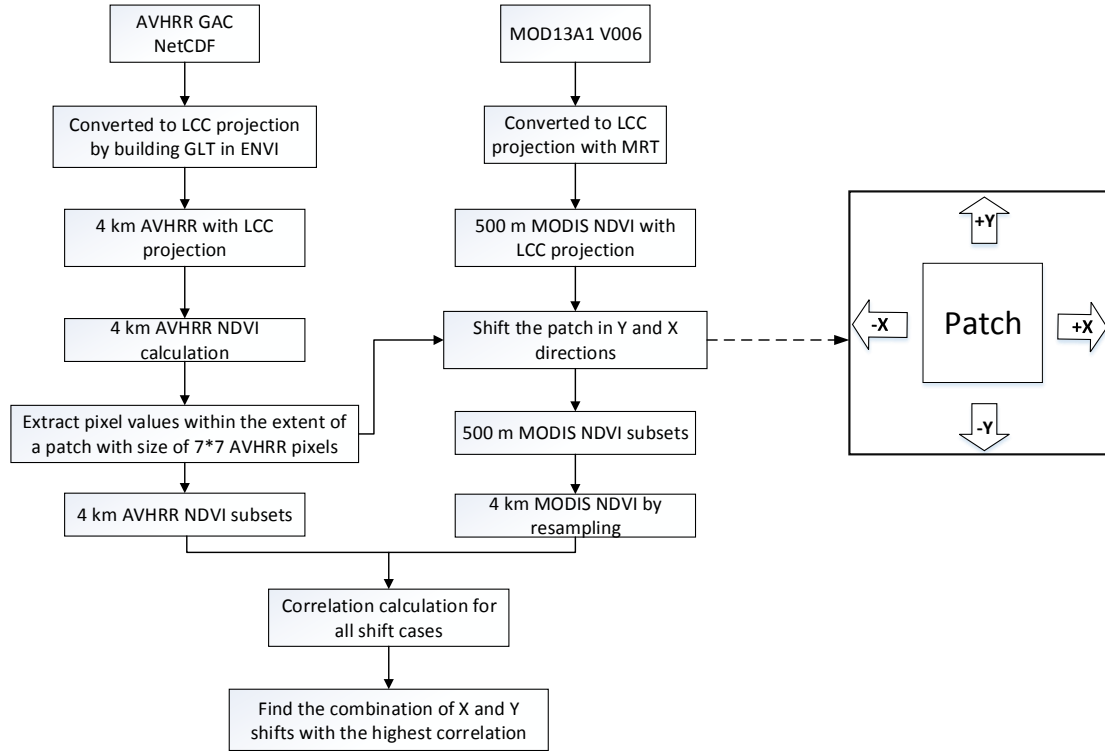
```
AVHRR GAC                          MOD13A1 V006
NetCDF

Converted to LCC projection        Converted to LCC
by building GLT in ENVI            projection with MRT

4 km AVHRR with LCC                 500 m MODIS NDVI with
projection                          LCC projection

4 km AVHRR NDVI                     Shift the patch in Y and X          Patch
calculation                         directions                         +Y  -X  +X  -Y

Extract pixel values within the extent of
a patch with size of 7*7 AVHRR pixels
                                    500 m MODIS NDVI subsets

4 km AVHRR NDVI subsets             4 km MODIS NDVI by
                                    resampling

            Correlation calculation for
            all shift cases

            Find the combination of X and Y
            shifts with the highest correlation
```

196

Figure 3. Flowchart of the Correlation-based Patch Matching Method (CPMM).

3.1 Satellite data processing

199   The AVHRR GAC data set is stored in a Network Common Data Format (NetCDF), with
200 latitude and longitude assigned to each pixel. In order to achieve a higher accuracy of image
201 matching, the data need to be reprojected. The AVHRR GAC scene was reprojected into the
202 Lambert Conformal Conic (LCC) projection by building the Geographic Lookup Table (GLT)
203 using the latitude and longitude data in ENVI. The spatial resolution of the AVHRR GAC map
204 in the LCC projection is 4 km. Based on the reprojected data, the NDVI was calculated using
205 the band combinations as indicated by Eq. (1). Similarly, the NDVI band of MOD13A1 in the
206 HDF format was extracted and converted to LCC projection from its raw sinusoidal projection
207 using the MODIS Reprojection Tool (MRT). The nearest neighbor (NN) resampling scheme
208 was employed in this procedure. The spatial resolution of the MODIS NDVI in the LCC
209 projection is 500 m. Thus, the geometric assessment is performed at the 4 km resolution of
210 AVHRR NDVI based on the 500 m MODIS NDVI data.

3.2 Patch matching and geometric assessment

212   In the process of matching the AVHRR GAC data with reference MODIS data, a patch
213 size of 7×7 AVHRR pixels (corresponding to approximately 28 km × 28 km) was used. These
214 patches were distributed in each ROI as shown in Figs. 1 and 2, with an interval of 4 pixels in
215 the along-track (Y-) and across-track (X-) direction. The sizes of the patch and interval were
216 determined based on the following aspects: the size of the patch should contain enough pixels
217 to support a robust correlation estimation, but at the same time, should not be too large in order

218 to investigate the potential influencing factors related to the geometric accuracy, and get enough
219 results from these patches to attain a more significant and comprehensive conclusion. Similarly,
220 the size of the interval should enable the disparity between different patches on one hand and
221 on the other hand a large number of patches within the extent of each ROI. The chosen size has
222 proven to be most ideal for these criteria during the test of different patch size.

223   For each patch in the ROI, the AVHRR GAC data within the patch were extracted. Then
224 the patch was shifted in the Y- and X-direction as indicated by the arrows in Fig. 3. Shifts were
225 conducted stepwise in order to achieve sub-pixel accuracy, beginning with only 500 m and
226 adding up to 8 km (i.e., ± 2 pixels) at a step of 500 m (equivalent to the MODIS pixel size) in
227 any direction of Y- and X-combination. Consequently, 33×33 combinations of X- and Y-shifts
228 have been simulated. For each simulated shift, the MODIS NDVI pixels within the extent of
229 the patch were extracted and aggregated to 4 km by spatial averaging. Afterwards, the
230 correlation between the 4 km rescaled MODIS NDVI and the 4 km AVHRR NDVI was
231 calculated for each shift in X- and Y-direction. The displacement of one patch was indicated by
232 the shift combination with the best correlation, which means the geolocation accuracy of the
233 patch. In this way, the geolocation errors were transformed into the across-track and along-track
234 directions at the sub-pixel level for correlation with possible error sources.

235   It is expected that the results from each patch are different. Therefore, the general accuracy
236 of each ROI was determined by summarizing the measured shifts of each respective patch
237 statistically. Here, the histogram was employed to show the distribution of geometric errors in
238 the across-track and along-track directions. And the quantitative indexes, such as the number
239 of patches, their mean and standard errors, were calculated. The averaging is expected to reduce
240 the uncertainties caused by random factors and produce accurate shift measurement estimates
241 (Bicheron et al., 2011). The final shifts of the scene were calculated by averaging the measured
242 shifts of all patches on the scene.

3.3 Influence factor

244   The influence of potential variables on the geometric accuracy was studied, including
245 SatZ, topography, latitudes, and longitude. To achieve this, the information of these factors were
246 also extracted for each patch on the scene. The geometric errors induced by SatZ were
247 highlighted by checking the relationship between errors and SatZ. The effect of topography
248 was investigated by checking the relationship of geometric errors in the across-track direction
249 over terrain areas compared to relatively flat areas. The effect of latitudes and longitude was
250 determined by analyzing their relationship with measured shifts on the along-track and across-
251 track directions, respectively.

4   Results and discussions

253   Fig. 4 shows the correlation distribution over the 33 × 33 simulated shifted cases within ±
254 8 km range at a step change of 500 m. Here, only one patch is extracted from each respective

scene to illustrate the results. Each grid in Fig. 4 represents a shift combination case, which is indicated by the location of the grid away from the center. The center of each subfigure depicts the case in which the location of the patch on the reference scene is exactly overlapped with that on the AVHRR scene. The results are visualized for one example showing the spatial distribution of correlation between the MODIS reference scene and the AVHRR data (Fig. 4). The color coding indicates a high correlation in dark green and reddish-white colors indicate low correlation values. It can be seen that the correlation appears a maximum at a certain location, and then becomes gradually smaller with increasing distance from that location. The location with the maximum correlation indicates the actual displacement of this patch. Then the geolocation errors can be transferred into distances in kilometer (km) by multiplying the location of the grid with 500 m. An almost perfect match is shown in Fig. 4b, where the dark green area is nearly centered at the coordinates (0, 0). From Fig. 4a, it can be found that the patch on the NOAA-17 scene shows geolocation errors of -1 km and 0 km in the along-track and across-track directions, respectively. The Fig. 4b indicates a geolocation error of 0 km and -0.5 km in the along-track and across-track directions respectively for the patch on the MetOp-A scene. And Fig. 4c indicates that the patch on the MetOp-B scene shows a geometric error of 2 km in the along-track direction and -5.5 km in the across-track direction. However, these figures show only the results of one single patch. The final results are based on a large number of samples to be statistically significant.
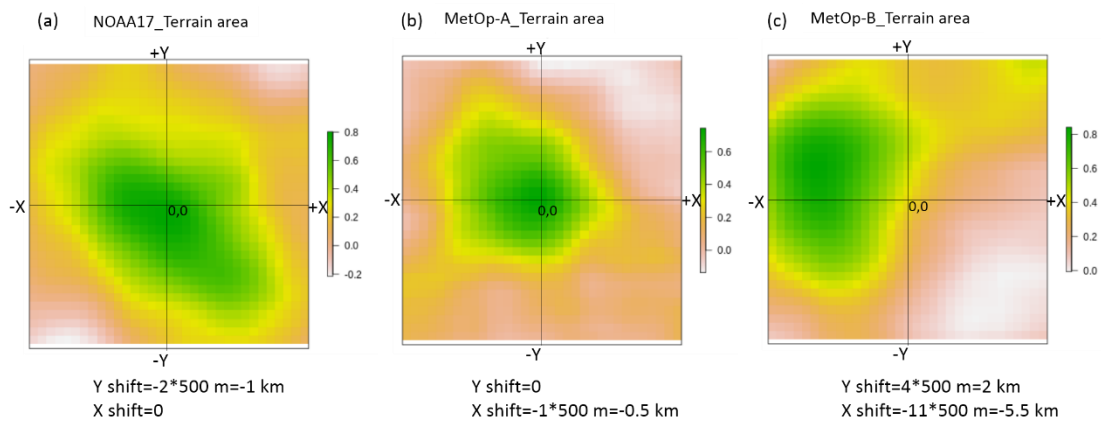

Figure 4. Variations of the correlation with respect to each shift combination. Only the results of one patch from the NOAA-17 (left), MetOp-A (middle), and MetOp-B (right) scenes are shown for conciseness.

4.1 Geocoding accuracy

The geolocation shifts of each patch are slightly different as shown in Figs. 5-7. The +y indicates a shift to the North and +x indicates a shift to the East (minus sign indicates opposite directions). The statistical indicators such as the mean value of shift (Mean), the standard deviation of shift (StdDev) and the number of patches (N), are derived from the estimated shift values of all patches within the extent of the corresponding ROI.

As shown in Fig. 5, it can be seen that the scene of NOAA-17 generally shows West shifts

in the across-track direction, since the majority of patches in all ROIs show negative shifts. Nevertheless, the magnitudes of shifts for different ROIs vary from one to another. ROI 2 shows the smallest shift with a mean value of -0.76 km, with most shifts concentrated around -1 (Fig. 5b). The ROIs 6 and 5 indicate the second smallest shifts, with still weak magnitudes of -1.33 and -1.35, respectively. Most of their shifts are distributed between -2 and 0 (Figs. 5f and e). The ROIs 7, 3, 1, 4 show slightly larger mean shifts but are still with the magnitudes of less than 2.5 km. These results are unexpected, because the ROIs (ROIs 2 and 6) over terrain areas are with smaller shifts than those (ROIs 7, 3, 1, 4) over relatively flat areas in the across-track direction. One possible reason is that the SatZ for ROIs 2 and 6 are not large (less than 40°) (Fig. 1b) so that the terrain effect on geolocation accuracy is counterbalanced by the small SatZ. This also indicates that the influence of small SatZ may be stronger than the terrain effect. But it is surprising that the ROI 7 (Fig. 5g), which is located at the nadir area (Fig. 1b), shows even larger shifts than other ROIs (ROIs 2, 6 and 5) with relatively larger SatZ. On the other hand, ROI 7 shows the most stable behavior, indicated by the smallest StdDev of 0.77. Other ROIs present relatively large, but still acceptable variations with StdDev ranging from 0.97 to 1.41 (Figs. 5a-g).

When combining the results of all ROIs together (Fig. 5h), the shifts in the across-track direction generally follow an approximately normal distribution with a mean value of -1.69 and a standard deviation of 1.32. Nearly 91% of the shifts are within the range of ± 3 km, and the great majority (97%) of the shifts lay within a range of ± 4 km. The number of patches (N=759) is assumed to be sufficient to ensure reliability and robustness of the results and the reduction of the influence of random factors.

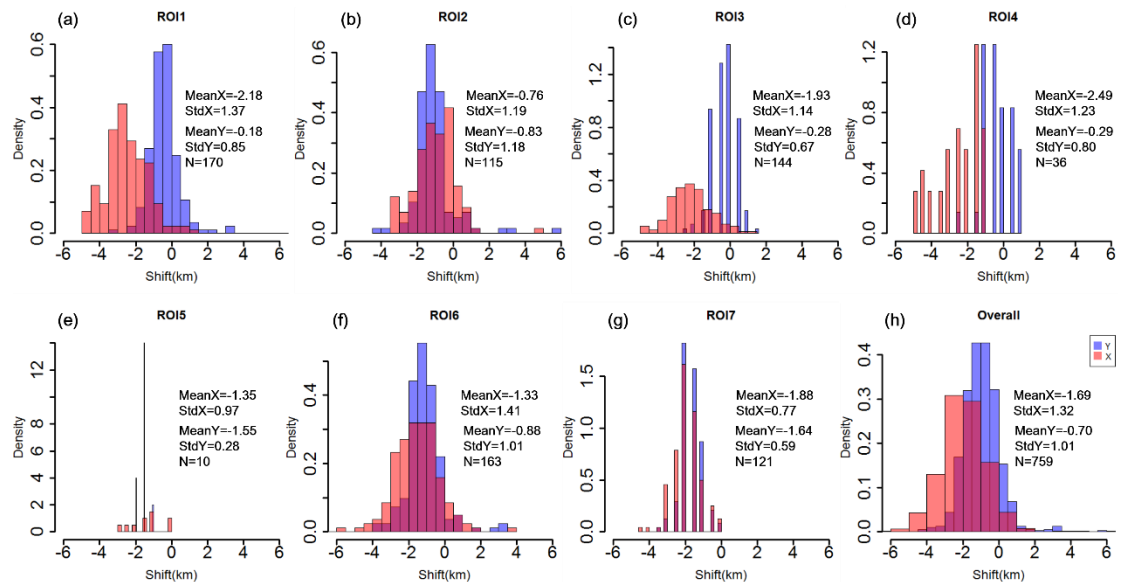**Figure 5.** The distribution of shifts in the across-track (X, represented by red histogram) and along-track (Y, denoted as blue histogram) directions over different regions for NOAA-17 scene. The unit of the shift is km. For histograms, the heights of the bars indicate the density. In this case, the area of each bar is the relative frequency, and the total area of the histogram is equal to 1.

312   The shifts in the along-track direction are mainly negative throughout these ROIs,
313   indicating that the NOAA-17 scene is dominated by South shifts in the along-track direction.
314   Nevertheless, a considerable number of patches also show slight North shifts over ROIs 1, 3
315   and 4 (Figs. 5a, c and d), where the shifts are distributed around 0 with mean values of -0.18, -
316   0.28 and -0.29, respectively. These shifts are generally small in these three regions given that
317   the maximum shift is no more than 3.5 km (Table 2). In contrast, the ROIs 2, 5, 6 and 7 present
318   systematic shifts to the South, which are mostly distributed within the range of -2 to 0 km, with
319   mean values of -0.83, -1.55, -0.88 and -1.64, respectively (Figs. 5b, e, f and g). The large
320   differences in the distribution of shifts over different ROIs demonstrate that the shifts in the
321   along-track direction are dependent on the region. It is interesting to find that ROI 7 still shows
322   the smallest StdDev of 0.59 when excluding ROI 5 due to its very small number of patches.
323   This indicates that ROI 7 also shows the smallest uncertainty in the along-track direction. And
324   this may be associated with its smallest SatZ among all investigated ROIs. When combining
325   the results of different ROIs (Fig. 5h), the overall shifts in the along-track direction
326   approximately obey a normal distribution, with an average of -0.70 and a standard deviation of
327   1.01. Nearly 70% of them are within the range of ± 1 km, and only a small part (1.5%) show
328   values larger than 3 km.

329   Furthermore, it can be stated that the distribution of shifts in the along-track direction is
330   less widely spread than that in the across-track direction, demonstrating the smaller uncertainty
331   of geocoding in the along-track direction, as indicated by the smaller StdDev values throughout
332   these ROIs (Table 2). Moreover, the geolocation errors in the across-track direction are greater
333   than the along-track direction (Fig. 5), which is expected due to the applied clock drift
334   correction.

335   **Table 2**. Summary of the results for the scene of NOAA-17. The unit of the shift is km.

ROI	Elevation(m)	Min(X)	Max(X)	Mean(X)	StdDev(X)	Min(Y)	Max(Y)	Mean(Y)	StdDev(Y)	N
1	481	-5	7	-2.18	1.37	-3.5	3.5	-0.18	0.85	170
2	1436	-3.5	5	-0.76	1.19	-4.5	6	-0.83	1.18	115
3	518	-5	1.5	-1.93	1.14	-2.5	1.5	-0.28	0.67	144
4	436	-5	-1	-2.49	1.23	-2.5	1	-0.29	0.80	36
5	543	-3	0	-1.35	0.97	-2	-1	-1.55	0.28	10
6	1094	-7.5	4	-1.33	1.41	-4	3.5	-0.88	1.01	163
7	440	-4.5	0	-1.88	0.77	-3.5	0	-1.64	0.59	121
Overall	/	-7.5	7	-1.69	1.32	-4.5	6	-0.70	1.01	759

336   Similar to the results of NOAA-17, MetOp-A scene mainly present West shifts in the
337   across-track direction, indicated by the widely distributed negative values throughout these
338   ROIs (Figs. 6a-f). These shifts are basically concentrated around -2, however, the ROIs 2 and
339   6 located in the terrain areas, show smaller average shifts (-1.68 and -1.82, respectively) than
340   those of ROIs 1 and 3 (-2.25 and -1.94, respectively) over the relatively flat areas. This is
341   understandable since the ROIs 2 and 6 are closer to the nadir area (Fig. 1d). And this align with
342   the results from NOAA-17, where the influence of SatZ is also stronger than the terrain effect.
343   Although the ROIs 5 and 4 show the smallest average shifts (-0.72 and -1.45, respectively) in

the across-track direction, their results may be biased due to the smaller number of analyzed patches. It is interesting to find that ROI 3, which is almost located in the nadir area, still shows the least uncertainty, indicated by the smallest StdDev of 0.67. Furthermore, all ROIs close to the nadir area are characterized by small StdDevs (0.8 and 1.03 for ROIs 2 and 6, respectively) compared to ROIs located further away from the nadir area (1.29, 2.05, 1.37 for ROIs 1, 4, 5, respectively). These results demonstrate that SatZ plays a crucial role in determining the uncertainty of the shifts in the across-track direction. This conclusion also agrees with previous research conducted by Aguilar et al. (2013). When combining the results of all ROIs (Fig. 6g), the shifts approximately follow a normal distribution, with an average of -1.90 and a standard deviation of 1.1. Most of the patches (94%) are within the range of ±3 km, and nearly 98% of them are with shifts less than ±4 km.

Since ROIs 1-6 on the MetOp-A scene are identical to those on NOAA-17 scene in terms of spatial extents, their shifts in the across-track direction are generally comparable. When excluding the results of ROIs 4 and 5, the ROIs on the MetOp-A scene generally show larger average shifts but smaller StdDevs than the NOAA-17 scene in the across-track direction (see Table 2 and 3). However, it does not necessarily mean that the MetOp-A scene has a smaller uncertainty than NOAA-17 scene in the across-track direction, because the ROIs on the MetOp-A scene are slightly closer to the nadir area than those on the NOAA-17 scene (Figs. 1b and d). Given the larger SatZ and the smaller average shifts of NOAA-17 scene, it is reasonable to conclude that the NOAA-17 scene shows a slightly better geolocation accuracy than the MetOp-A scene in the across-track direction.
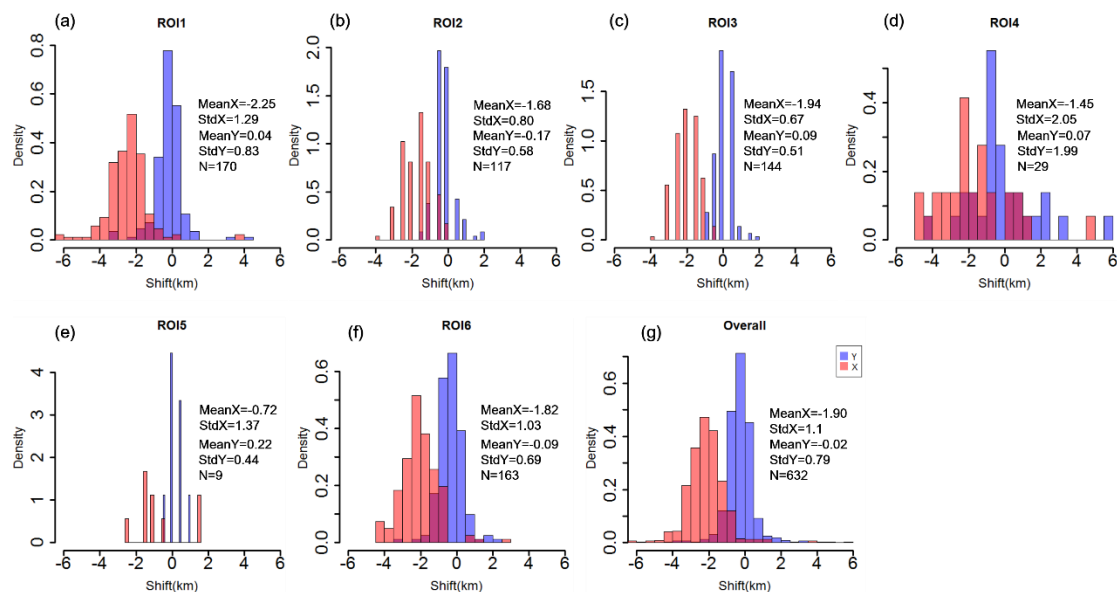

Figure 6. The distribution of shifts in the across-track (X, represented by red histogram) and along-track (Y, denoted as blue histogram) directions over different regions for MetOp-A scene. The unit of the shift is km. For histograms, density instead of frequency is labelled in the ordinate.

Looking at the shifts in the along-track direction, the MetOp-A scene does not show strong

370 systematic North or South shifts, but rather a general distribution of the shifts around 0 (Figs.

371 6a-f). The shifts are generally small within a range of ± 1 km, with StdDevs less than 0.83

372 except for ROI 4. Furthermore, ROIs 2, 3 and 6 that are located close to the nadir area exhibit

373 smaller StdDevs than those located further away from the nadir area when excluding ROI 5 due

374 to its very small number of patches. This further indicates that SatZ also determines the

375 uncertainty of shifts in the along-track direction. When combining the results of all ROIs (Fig.

376 6g), the shifts also display a nearly normal distribution, with an average of -0.02 and a StdDev

377 of 0.79. Nearly 94% of the shifts are within the range of ± 1 km and almost all of them (98%)

378 are distributed within the range of ± 2 km. It can be found that the shifts in the along-track

379 direction are obviously smaller and more centralized than those in the across-track direction.

380 This can be further confirmed by the consistently smaller StdDev values in the along-track

381 direction than those in the across-track direction as shown in Table 3.

382 **Table 3**. Summary of the results for the scene of MetOp-A. The unit of the shift is km.

ROI	Elevation(m)	Min(X)	Max(X)	Mean(X)	StdDev(X)	Min(Y)	Max(Y)	Mean(Y)	StdDev(Y)	N
1	479	-7	4	-2.25	1.29	-3.5	4.5	0.04	0.83	170
2	1440	-4	0	-1.68	0.80	-1.5	2	-0.17	0.58	117
3	518	-4	-0.5	-1.94	0.67	-1	2	0.09	0.51	144
4	436	-5	5	-1.45	2.05	-4.5	6	0.07	1.99	29
5	540	-2.5	1.5	-0.72	1.37	-0.5	1	0.22	0.44	9
6	1095	-4.5	3	-1.82	1.03	-3.5	2.5	-0.09	0.69	163
Overall	/	-7	5	-1.90	1.10	-4.5	6	-0.02	0.79	632

383 By comparing Figs. 6a-f with Figs. 5a-f, it becomes obvious that large differences exist

384 between the shifts in the along-track direction of MetOp-A and NOAA-17 scenes. In the first

385 place, systematic South shifts occur on the NOAA-17 scene but not on the MetOp-A scene.

386 Secondly, the magnitudes of shifts on the MetOp-A scene are generally smaller than those on

387 the NOAA-17 scene, as the former are concentrated around 0 while the latter are concentrated

388 around -1. Thirdly, the distribution of shifts is more centralized for the MetOp-A scene

389 compared to the NOAA-17 scene, except for ROIs 4 and 5. This can further be proved by the

390 smaller StdDev values for MetOp-A (Table 3) than those for NOAA-17 (Table 2). Therefore, it

391 can be concluded that the MetOp-A scene shows a better geolocation accuracy and less

392 uncertainty than the NOAA-17 scene in the along-track direction.

393 Similar to the scenes of NOAA-17 and MetOp-A, the MetOp-B scene generally shows

394 West shifts in the across-track direction, indicated by the predominant occurrence of negative

395 values (Figs. 7a-f). Nevertheless, unlike the results for the terrain areas on NOAA-17 and

396 MetOp-A scenes, the ROI c located in the terrain area on the MetOp-B scene (Fig. 2a), shows

397 the largest shifts throughout these ROIs with an average of -4.69 in the across-track direction.

398 Furthermore, the magnitudes of these shifts are characterized by even larger values than 6 km

399 (Fig. 7c). This is most probably caused by the combined effect of topography and large SatZ

400 (Fig. 2b). Significant terrain effects appear only in the case of SatZ larger than 40° as shown in

Fig. 2b. This finding agrees with the previous study by Fontana et al. (2009), who demonstrated that the errors in across-track direction result from the intertwined effects of observation geometry and terrain elevation. Nevertheless, ROI e that is located in the nadir area (Fig. 2d), shows the smallest average shift of -1.29 but the largest standard deviation of 2.51 (Fig. 7e). The largest StdDev is attributed to the fact that a considerable number of shifts exhibit values of ± 6 km. As shown in Fig. 2c, the main reason for these large and unstable shifts may be the presence of thin clouds or cloud shadows in this region. By comparing the results of ROIs d and e with smaller SatZ against ROIs b, c, f with larger SatZ (Figs. 2b and d), it can be stated that the shifts with smaller SatZ are generally weaker than those with larger SatZ (Figs. 7b-f). When combining the results of all ROIs (Fig. 7g), the MetOp-B scene shows an average shift of -2.56 km with a standard deviation of 2.19 in the across-track direction. Only 63% of the shifts are distributed within the range of ± 3 km, and the percentage raises up to 92% within the range of ± 5.5 km.
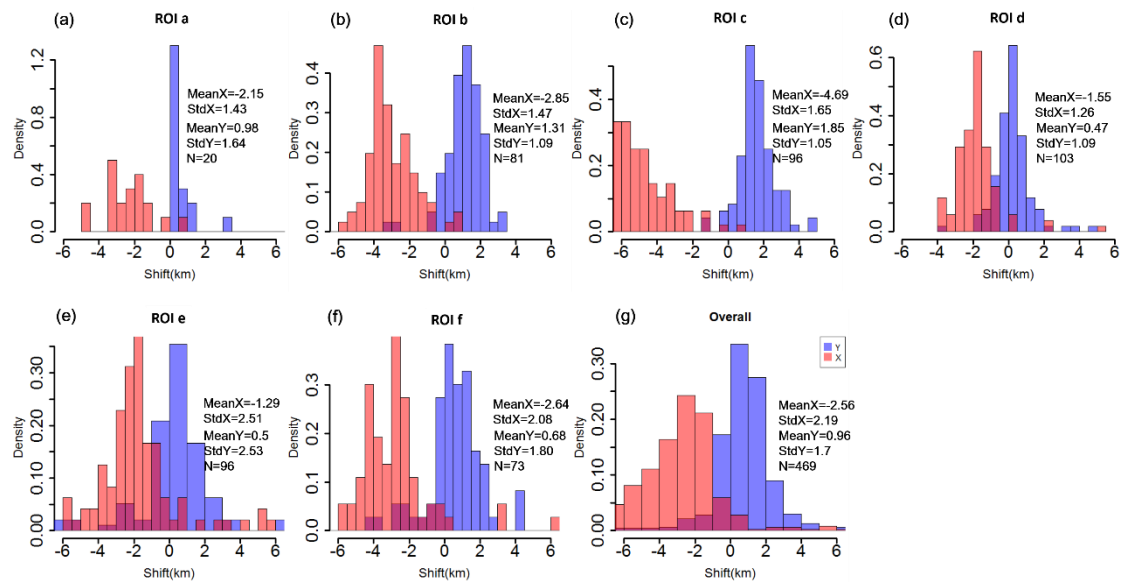

Figure 7. The distribution of shifts in the across-track (X, represented by red histogram) and along-track (Y, denoted as blue histogram) directions over different regions for MetOp-B scene. The unit of the shift is km. For histograms, density instead of frequency is labelled in the ordinate.

Since the extent of the ROIs in the MetOp-B scene are not consistent with those on NOAA-17 and MetOp-A scenes, only their overall performances in the across-track direction are compared here. By comparing Fig. 7g with Fig. 6g and Fig. 5h, it is obvious that the MetOp-B scene shows larger shifts and greater uncertainties than NOAA-17 and MetOp-A scenes in the across-track direction. This is partly due to the larger range of SatZ of these ROIs and partly due to the worse geolocation accuracy of the MetOp-B scene in the across-track direction.

The MetOp-B scene is dominated by North shifts in the along-track direction, indicated by the predominantly positive shift values (Figs. 7a-f). It is interesting to find that ROI c, which is located at terrain area and with large SatZ, shows the largest shifts with an average of 1.85

427 km in the along-track direction. Given that terrain does not affect the geolocation accuracy in
428 the along-track direction, the main cause of the largest shift may be the largest SatZ of ROI c
429 among these ROIs. Furthermore, by comparing the results of ROI d and e with those of ROI b,
430 c, f, it can be found the shifts of ROIs with smaller SatZ are more concentrated around 0 (Figs.
431 7d and e), while the shifts of ROIs with larger SatZ are more widely spread (Figs. 7b, c, and f).
432 This manifests that the effect of large SatZ on shifts in the along-track direction cannot be
433 neglected. When combining the results of all ROIs, the MetOp-B scene shows shifts with an
434 average of 0.96 and a standard deviation of 1.7. Only 52% of the shifts are distributed within
435 the range of ± 1 km, and the percentage raises up to 92% for the range of ± 3 km.

436   It can be seen that the shifts in the along-track direction are still significantly smaller than
437 those in the across-track direction. Furthermore, the uncertainties of the shifts in the along-track
438 direction are generally smaller than those in the across-track direction, when excluding the
439 results of ROI a due to its limited number of patches (Table 4). This further verifies that after
440 removing clock drift errors, the geolocation errors in the along-track direction are generally
441 more accurate and with less uncertainties than the across-track direction.

442 **Table 4**. Summary of the results for the scene of MetOp-B. The unit of the shift is km.

ROI	Elevation(m)	Min(X)	Max(X)	Mean(X)	StdDev(X)	Min(Y)	Max(Y)	Mean(Y)	StdDev(Y)	N
a	236	-5	1	-2.15	1.43	0	7	0.98	1.64	20
b	566	-7.5	1	-2.85	1.47	-3.5	3.5	1.31	1.09	81
c	1677	-7.5	1	-4.69	1.65	-1.5	5	1.85	1.05	96
d	406	-4	5.5	-1.55	1.26	-4	5	0.47	1.09	103
e	729	-6	7.5	-1.29	2.51	-7.5	7.5	0.50	2.53	96
f	420	-7.5	6.5	-2.64	2.08	-7	4.5	0.68	1.80	73
Overall	/	-7.5	7.5	-2.56	2.19	-7.5	7.5	0.96	1.70	469

443   The comparison of Fig. 7g with Fig. 6g and Fig. 5h reveals that the MetOp-B scene is
444 significantly inferior to the MetOp-A scene in terms of the geolocation accuracy in the along-
445 track direction, with the former being concentrated around 1 and the latter around 0.
446 Furthermore, the uncertainty of the shifts of the MetOp-B scene (StdDev=1.7) is much larger
447 than that of the MetOp-A scene (StdDev=0.79). As for the performance of the MetOp-B scene
448 relative to the NOAA-17 scene, it can be found that they are comparable with regard to the
449 magnitude as well as the distribution of the shifts in the along-track direction. However, the
450 MetOp-B scene shows larger uncertainties than NOAA-17.

451   From the results above, it can be concluded that NOAA-17 and MetOp-A scenes show
452 distinct advantages over the MetOp-B scene in both directions. However, the NOAA-17 scene
453 is slightly better than the MetOp-A scene in the across-track direction, with average shifts of -
454 1.69 for NOAA-17 and -1.90 for MetOp-A, which are both greatly lower than for MetOp-B (-
455 2.56). But the MetOp-A scene shows a distinct advantage over NOAA-17 in the along-track
456 direction, with an average shift of -0.02 for MetOp-A and -0.7 for NOAA-17, which are both
457 lower than for MetOp-B (0.96). In addition to the magnitudes of their shifts, the MetOp-B scene
458 also shows larger uncertainties than NOAA-17 and MetOp-A scenes in both directions.

4.2 The potential influence factors

459

460   From the above results, it is known that SatZ plays an important role in determining the
461   geolocation accuracy of the satellite scene. To investigate how and to what extent it influences
462   the geolocation accuracy, Fig. 8 displays the shifts in both directions as a function of SatZ for
463   all three satellites. Furthermore, the influences of latitude and longitude on geolocation
464   accuracy are also explored.

465   As shown in Figs. 8a-c, it can be seen that the shifts in the across-track direction vary
466   considerably for all SatZ, and this is particularly evident in the results of MetOp-B (Fig. 8c).
467   This demonstrates that besides the SatZ effects, the geolocation accuracy is also influenced by
468   other factors. Furthermore, the spread at each fixed SatZ tends to become larger at larger SatZ
469   (larger than 20°) (Figs. 8a-b). The large variability of MetOp-B scene shifts at small SatZ (less
470   than 20°) (Fig. 8c) is mainly due to the effect of thin cloud or cloud shadow as explained before.
471   Despite the dispersion of the shifts for all SatZ, it can still be found that the shifts in the across-
472   track direction do not change much when the SatZ is less than 20° (Figs. 8a-b and Table 5). A
473   slightly decreasing trend (increasing trend of the magnitude) can be observed from 20° to 40°
474   (Table 5), and becomes more apparent at SatZ larger than 40° (Fig. 8c and Table 5).
475   Furthermore, it can be found that for small SatZ (less than 20°) the shifts in the across-track
476   direction are generally concentrated around 2 km for NOAA-17 and MetOp-A scenes (Figs. 8a-
477   b). With increasing SatZ, the largest magnitudes of shifts become larger but basically stay
478   within the range of 4 km for SatZ smaller than 40°. For even larger SatZ (larger than 40°), the
479   magnitude of shifts can reach 6 km for NOAA-17 scene and 8 km for MetOp-B scene. From
480   these results, it can be inferred that the SatZ has a considerable effect on both the magnitude
481   and uncertainty of the shifts in across-track direction. The larger SatZ generally contributes to
482   larger shifts and uncertainties in the across-track direction. Furthermore, it can be inferred that
483   the GAC data with SatZ less than 40° should be preferred in applications.

484   Compared to the shifts in the across-track direction (Figs. 8a-c), the shifts in the along-
485   track direction show smaller variability at each fixed SatZ (Figs. 8d-f). From Figs. 8d-e, it can
486   be seen that the shifts in the along-track direction are relatively stable at each level of SatZ for
487   SatZ smaller than 15°, but becomes more variable for greater SatZ. A similar phenomenon can
488   be observed in Fig. 8f, where the shifts are relatively stable with SatZ ranging from 20° to 35°,
489   but becomes more variable at each level of SatZ with its values larger than 35°. It is noteworthy
490   that the wide spread of shifts with SatZ less than 20° is mainly caused by cloud contamination.
491   These results confirm the influence of larger SatZ on the uncertainty of shifts in the along-track
492   directions. It is interesting to find that the magnitudes of NOAA-17 scene shifts with small SatZ
493   (less than 20°) are even larger than those with larger SatZ (larger than 20°) (Fig. 8d). On the
494   contrary, the magnitudes of MetOp-B scene shifts with smaller SatZ (20-35°) are smaller than
495   those with larger SatZ (larger than 35°) (Fig. 8f). Nevertheless, all three sensors have in
496   common that they do not show clear change with SatZ smaller than 20° for NOAA-17 and

497 smaller than 35° for MetOp-A and MetOp-B (Figs. 8d-f). For larger SatZ than these values,

498 shifts exhibit a slightly decreasing trend for NOAA-17 (Fig. 8d) and an increasing trend for

499 MetOp-B (Fig. 8f). From these results, it can be stated that the influences of large SatZ on the

500 magnitude of shifts in the along-track direction are probably intertwined with other factors.
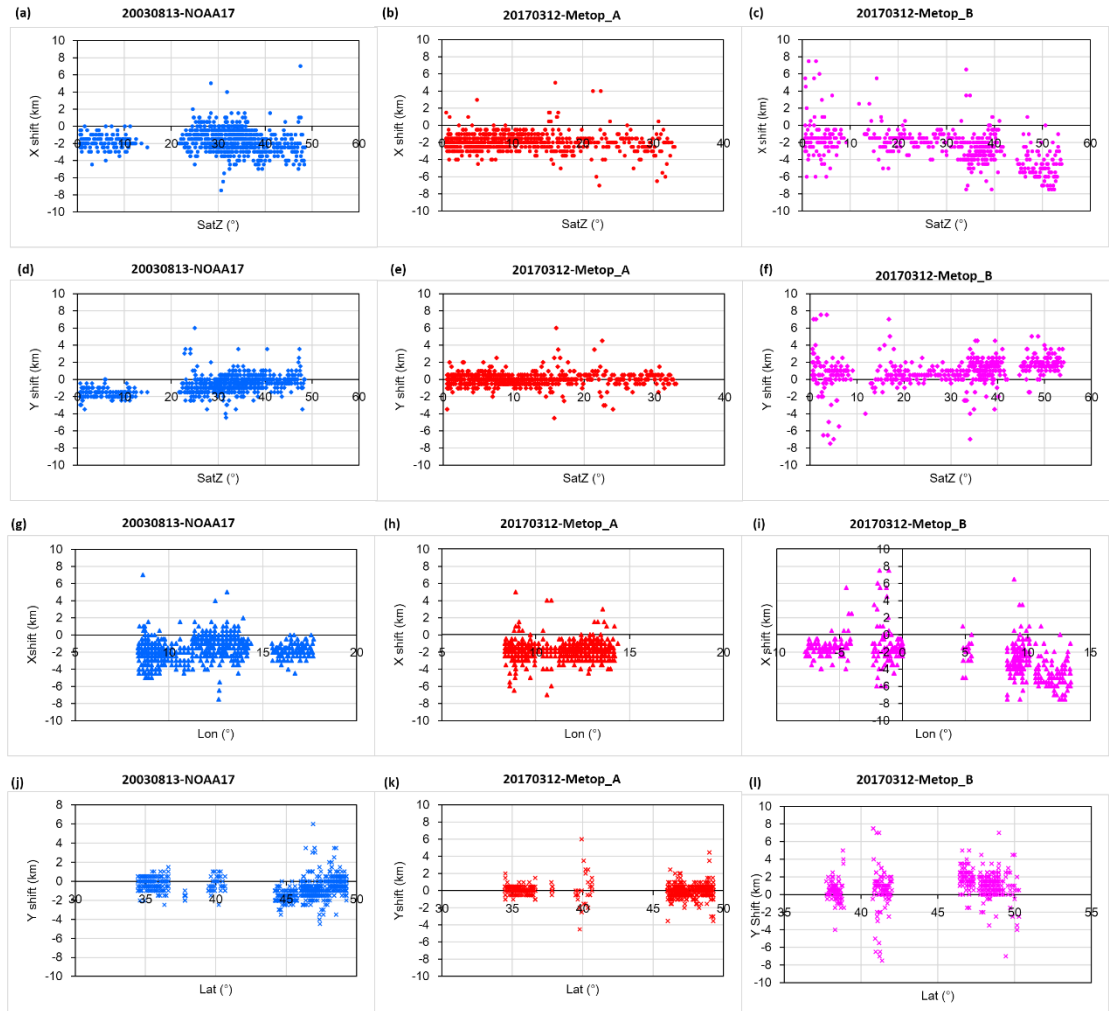

501

Figure 8. Influence of SatZ on the geolocation accuracy in the across-track (a-c) and along-track (d-f)
directions. (g-i) and (j-l) describe the influence of longitude and latitude on the geolocation accuracy in
the across-track and along-track directions, respectively. The left column indicates results of NOAA-17
(blue), middle for MetOp-A (red), and right for MetOp-B (pink) scenes.

Table 5. The mean shift for each range of SatZ in the across-track direction. The unit of the shift is km.

SatZ	0°-10°	10°-20°	20°-30°	30°-40°	40°-50°	50°-60°
NOAA-17	-1.84	-1.84	-1.32	-1.66	-2.27	
MetOp-A	-1.87	-1.80	-2.06	-2.62		
MetOp-B	-1.29	-1.45	-1.75	-2.71	-3.95	-4.93

507 For NOAA-17, the shifts tend to be smaller with the longitudinal range of 10°-15° and

508 become larger outside this range (Fig. 8g). The MetOp-A scene does not show apparent change

509 with longitude between 8° and 15° and neither does MetOp-B within the range between -8° and

0° (Fig. 8 h and i, respectively). However, MetOp-B presents a clear decreasing trend (an increasing trend in magnitude) for longitudes larger than 5°. Given the fact that the latitude of the nadir area is distributed between 10°-15° for NOAA-17, 8°-15° for MetOp-A, and -8°-0° for MetOp-B (Figs. 1b and d, Figs. 2b and d), it can be concluded that the influence of longitude on the shifts in the across-track direction is related to the longitude of nadir area of the satellite, as it shows almost no influence in the nadir area. The influence increases with the difference of the longitude relative to that of the nadir area. This is well understandable, as the influence of longitude is equivalent to that of SatZ in the across-track direction.

The variation of the shifts (in the along-track direction) with latitude also depends on the situation (Figs. 8j-l). The magnitudes of shifts with larger latitude (larger than 45°) are generally greater than those with smaller latitude (less than 40°) on the NOAA-17 (Fig. 8j) and MetOp-B scene (Fig. 8l). This is not visible for the MetOp-A scene (Fig. 8k), where the shifts exhibit almost no change with latitude. This can be attributed to the fact that the clock drift errors are corrected more thoroughly for MetOp-A satellite than NOAA-17 and MetOp-B satellites. Furthermore, the MetOp satellites have an on-board stabilization to keep them in the right position and orientation in orbit compared to the NOAA satellites.

5 Conclusions

The geometric accuracy of satellite data is crucial for most applications as geometric inaccuracy can bias the obtained results. Therefore, the assessment of the geolocation accuracy is important to provide satellite data of high quality enabling successful applications. In this study, a correlation-based patch matching method was proposed to characterize and quantify the AVHRR GAC geo-location accuracy. This method presented here yields significant advantages over existing approaches and enables achieving a subpixel geo-positioning accuracy of coarse resolution scenes. It is free from the impact of false detection due to the influence of mixed pixels, not limited to a certain landmark (e. g. shoreline) and therefore enables a more comprehensive geometric assessment. This method was utilized to characterize the geolocation accuracy of AVHRR GAC scenes from NOAA-17, MetOp-A, and MetOp-B satellites.

The study is based on several ROIs comprising numerous patches over different land cover types, latitudes, and topographies. The scenes from these satellites all present West shifts in the across-track direction, with an average shift of -1.69 km and a StdDev of 1.32 km for NOAA-17, -1.9 km and 1.1 km respectively for MetOp-A, and -2.56 km and 2.19 km respectively for MetOp-B. In regard to the shifts in the along-track direction, NOAA-17 generally shows South shifts with an average of -0.7 km and a StdDev of 1.01 km. By contrast, the MetOp-B mainly present North shifts with an average of 0.96 km and a StdDev of 1.70 km. The MetOp-A scene shows a distinct advantage over NOAA-17 and MetOp-B in the along-track direction without obvious shifts, indicated by the average of -0.02 km and a StdDev of 0.79 km. Generally, the MetOp-B scene is inferior to NOAA-17 and MetOp-A scenes, with larger shifts and

547 uncertainties in both directions. Despite the variation of shifts due to various factors (e. g. SatZ,
548 topography), more than 90 percent of the AVHRR GAC data across-track errors are within $\pm$
549 3 km for NOAA-17 and MetOp-A, and $\pm$5.5 km for MetOp-B. Along-track errors are within
550 $\pm$2 km for NOAA-17, $\pm$1 km for MetOp-A, and $\pm$3 km for MetOp-B for more than 90
551 percent of the test data. It is important to note that since these satellites show different shifts,
552 using the combined data from NOAA-17 and MetOp will result in additional uncertainty in
553 time series applications.

554 From the results above, it can be found that the geolocation accuracy in the along-track
555 direction is always higher and with less uncertainties than the across-track direction, which is
556 consistent with previous related studies. This is understandable since the GAC dataset from the
557 ESA cloud CCI project has been corrected for clock drift errors, but has no ortho-correction,
558 which is not feasible due to the onboard sampling characteristics. SatZ plays a decisive role in
559 determining the magnitude as well as the uncertainty of the shifts in the across-track direction.
560 Larger SatZ generally induce greater shifts and uncertainties in this direction. The combined
561 effect of SatZ and topography on geolocation accuracy in the across-track direction has also
562 been shown. And significant terrain effects appear only in the case of large SatZ (>40° for this
563 study). It is important to note that the effect of SatZ on the magnitude and uncertainty of shifts
564 in the along-track direction is not negligible. But this effect is likely to be intertwined with other
565 factors. The impact of longitude on the shifts in the across-track direction is equivalent to that
566 of SatZ, while the effect of latitude is related to the degree of how the clock drift errors are
567 corrected. It was found that the clock drift errors are more thoroughly corrected for MetOp-A
568 than NOAA-17 and MetOp-B.

569 Although this assessment was only conducted for a single scene of each satellite, the
570 highly variable ROIs take the influential factors of geometric accuracy well into account.
571 Therefore, the presented conclusions are transferable to other regions or seasons. However, it
572 is noteworthy that this method is not applicable to homogeneous surface (e.g., water, desert),
573 where the correlations are almost the same in any simulated displacement cases. In general, this
574 study provides an important preliminary geolocation assessment for AVHRR GAC data. It is a
575 first step towards a more precise geolocation and thus improves application of coarse-resolution
576 satellite data. For instance, it identifies the threshold of SatZ under which the GAC data should
577 be preferred in applications. Furthermore, the CPMM geolocation assessment method proposed
578 by this study is also applicable to other coarse-resolution satellite data.

Data availability

580 The AVHRR GAC test data in this paper draw on datasets from ESA CCI cloud project
581 (http://www.esa-cloud-cci.org/) where is also the data availability indicated (Stengel et al.,
582 2017). And the MOD13A1 V006 data can be downloaded via
583 https://ladsweb.modaps.eosdis.nasa.gov/ (Didan, 2015).

Author contributions

Xiaodan Wu was responsible for the main research ideas and writing the manuscript. Kathrin Naegeli contributed to the data collection. Stefan Wunderle contributed to the manuscript organization. All the authors thoroughly reviewed and edited this paper.

Competing interests

The authors declare that they have no conflict of interest.

Acknowledgments

References

Aguilar, M. A., del Mar Saldana, M., and Aguilar, F. J.: Assessing geometric accuracy of the orthorectification process from GeoEye-1 and WorldView-2 panchromatic images, Int. J. Appl. Earth Obs., 21, 427-435, 2013.

Aksakal, S. K.: Geometric accuracy investigations of SEVIRI high resolution visible (HRV) level 1.5 Imagery, Remote Sens., *5*(5), 2475-2491, 2013.

Aksakal, S. K., Neuhaus, C., Baltsavias, E., and Schindler, K.: Geometric quality analysis of AVHRR orthoimages, Remote Sens., *7*(3), 3293-3319, 2015.

Alcaraz‑Segura, D., Chuvieco, E., Epstein, H. E., Kasischke, E. S., and Trishchenko, A.: Debating the greening vs. browning of the North American boreal forest: differences between satellite datasets, Global Change Biol., 16(2), 760-770, 2010.

Arnold, G. T., Hubanks, P. A., Platnick, S., King, M. D., and Bennartz, R.: Impact of Aqua misregistration on MYD06 cloud retrieval properties. In Proceeding of MODIS Science Team Meeting, Washington, DC, USA, 26–28 January 2010.

Bennartz, R.: On the use of SSM/I measurements in coastal regions. J. Atmos. Oceanic Technol., 16(4), 417-431, 1999.

Bicheron, P., Amberg, V., Bourg, L., Petit, D., Huc, M., Miras, B., ... and Leroy, M.: Geolocation Assessment of MERIS GlobCover Orthorectified Products, IEEE Trans. Geosci. Remote Sens., 49(8), 2972-2982, 2011.

Cihlar, J., Latifovic, R., Chen, J., Trishchenko, A., Du, Y., Fedosejevs, G., and Guindon, B.: Systematic corrections of AVHRR image composites for temporal studies, Remote Sens. Environ., 89(2), 217-233, 2004.

Delbart, N., Le Toan, T., Kergoat, L., and Fedotova, V.: Remote sensing of spring phenology in

boreal regions: A free of snow-effect method using NOAA–AVHRR and SPOT–VGT data (1982–2004), Remote Sens. Environ., 101, 52−62, 2006.

Devasthale, A., Raspaud, M., Schlundt, C., Hanschmann, T., Finkensieper, S., Dybbroe, A., ... and Karlsson, K. G.: PyGAC: an open-source, community-driven Python interface to preprocess more than 30-year AVHRR Global Area Coverage (GAC) data, 2016.

Dietz, A. J., Frey, C. M., Ruppert, T., Bachmann, M., Kuenzer, C., and Dech, S.: Automated Improvement of Geolocation Accuracy in AVHRR Data Using a Two-Step Chip Matching Approach—A Part of the TIMELINE Preprocessor, Remote Sens., 9(4), 303, 2017.

Didan, K.: MOD13A1 MODIS/Terra Vegetation Indices 16-Day L3 Global 500m SIN Grid V006 [Data set], NASA EOSDIS LP DAAC, doi: 10.5067/MODIS/MOD13A1.006, https://ladsweb.modaps.eosdis.nasa.gov/, 2015.

D'Souza, G., and Malingreau, J. P.: NOAA‑AVHRR studies of vegetation characteristics and deforestation mapping in the Amazon Basin, Remote Sens. Rev., 10(1-3), 5-34, 1994.

Fontana, F. M., Trishchenko, A. P., Khlopenkov, K. V., Luo, Y., and Wunderle, S.: Impact of orthorectification and spatial sampling on maximum NDVI composite data in mountain regions, Remote Sens. Environ., 113(12), 2701-2712, 2009.

WMO, I., and UNEP, I.: Systematic observation requirements for satellite-based products for climate-Supplemental details to the satellite-based component of the "Implementation Plan for the Global Observing System for Climate in Support of the UNFCCC"[J]. Technical Report GCOS-107, WMO/TD No 1338, 2006.

Han, Y., Weng, F., Zou, X., Yang, H., and Scott, D.: Characterization of geolocation accuracy of Suomi NPP advanced technology microwave sounder measurements. J. Geophys. Res. Atmos., 121(9), 4933-4950, 2016.

Hoffman, L. H., Weaver, W. L., and Kibler, J. F.: Calculation and accuracy of ERBE scanner measurement locations, NASA Tech. Pap. Rep. NASA/TP-2670, 34 pp., NASA Langley Research Center, Hampton, Virginia, 1987.

Hollmann, R., Merchant, C., Saunders, R., Downy, C., Buchwitz, M., Cazenave, A., Chuvieco, E., Defourny, P., Leeuw, G. de, Forsberg, R., Holzer-Popp, T., Paul, F., Sandven, S., Sathyendranath, S., Roozendael, M. van, and Wagner W.: The ESA Climate Change Initiative: satellite data records for essential climate variables, B. Am. Meteorol. Soc., doi: 10.1175/BAMS-D-11-00254.1, 2013.

Hori, M., Sugiura, K., Kobayashi, K., Aoki, T., Tanikawa, T., Kuchiki, K., ... and Enomoto, H.: A 38-year (1978–2015) Northern Hemisphere daily snow cover extent product derived using consistent objective criteria from satellite-borne optical sensors, Remote Sens. Environ., 191, 402-418, 2017.

Khlopenkov, K. V., Trishchenko, A. P., and Luo, Y.: Achieving subpixel georeferencing accuracy in the Canadian AVHRR processing system, IEEE Trans. Geosci. Remote Sens., 48(4), 2150-2161, 2010.

Kidwell, K. B.: NOAA Polar Orbiter Data (POD) User's Guide, November 1998 revision, 1998.

http://www2.ncdc.noaa.gov/docs/podug/

Lee, T. Y., and Kaufman, Y. J.: Non-Lambertian effects on remote sensing of surface reflectance and vegetation index, IEEE Trans. Geosci. Remote Sens., 24, 699−708, 1986.

Moreno, J. F., and Melia, J.: A method for accurate geometric correction of NOAA AVHRR HRPT data, IEEE Trans. Geosci. Remote Sens., 31(1), 204-226, 1993.

Moulin, S., Kergoat, L., Viovy, N., and Dedieu, G.: Global-scale assessment of vegetation phenology using NOAA/AVHRR satellite measurements, J. Climate, 10, 1154−1170, 1997.

Pouliot, D., Latifovic, R., and Olthof, I.: Trends in vegetation NDVI from 1 km AVHRR data over Canada for the period 1985–2006, Int. J. Remote Sens., 30, 149−168, 2009.

Rosborough, G. W., Baldwin, D. G., and Emery, W. J.: Precise AVHRR image navigation, IEEE Trans. Geosci. Remote Sens., 32(3), 644-657, 1994.

Stengel, M., Stapelberg, S., Sus, O., Schlundt, C., Poulsen, C., Thomas, G., Christensen, M., Carbajal Henken, C., Preusker, R., Fischer, J., Devasthale, A., Willén, U., Karlsson, K.-G., McGarragh, G. R., Proud, S., Povey, A. C., Grainger, R. G., Meirink, J. F., Feofilov, A., Bennartz, R., Bojanowski, J. S., and Hollmann, R.: Cloud property datasets retrieved from AVHRR, MODIS, AATSR and MERIS in the framework of the Cloud_cci project, Earth Syst. Sci. Data, 9, 881-904, https://doi.org/10.5194/essd-9-881-2017, 2017.

Stengel, M., Sus, O., Stapelberg, S., Schlundt, C., Poulsen, C., Hollmann, R.: ESA Cloud Climate Change Initiative (ESA Cloud_cci) data: Cloud_cci AVHRR-AM L3C/L3U CLD_PRODUCTS v2.0, Deutscher Wetterdienst (DWD), https://doi.org/10.5676/DWD/ESA_Cloud_cci/AVHRR-AM/V002, 2017

Stöckli, R., and Vidale, P. L.: European plant phenology and climate as seen in a 20 year AVHRR land-surface parameter dataset, Int. J. Remote Sens., 25, 3303−3330, 2004.

Takagi, M.: Precise geometric correction for NOAA and GMS images considering elevation effects using GCP template matching and affine transform, Proceedings of SPIE Conference on Remote Sensing, Image and Signal Processing for Remote Sensing IX, pp.132-141, Vol. 5238, Barcelona, Spain, 2004.

Van, A., Nakazawa, M., and Aoki, Y.: Highly accurate geometric correction for NOAA AVHRR data, 2008. http://cdn.intechopen.com/pdfs/10391/InTech%20Highly_accurate_geometric_correction_for_noaa_avhrr_data.pdf

Wang, L., Tremblay, D. A., Han, Y., Esplin, M., Hagan, D. E., Predina, J., Suwinski, L., Jin, X., and Chen, Y.: Geolocation assessment for CrIS sensor data records. J. Geophys. Res. Atmos., 118(22), 12-690, 2013.

Wolfe, R. E., Nishihama, M., Fleig, A. J., Kuyper, J. A., Roy, D. P., Storey, J. C., and Patt, F. S.: Achieving sub-pixel geolocation accuracy in support of MODIS land science, Remote Sens. Environ., 83(1-2), 31-49, 2002.

Wolfe, R. E., Lin, G., Nishihama, M., Tewari, K. P., Tilton, J. C., and Isaacman, A. R.: Suomi NPP VIIRS prelaunch and on-orbit geometric calibration and characterization, J. Geophys. Res.

695   Atmos., 118, 11,508–11,521, 2013.